UILU-ENG 87-3601

Report No. 135

STRUCTURE/CHEMISTRY/PROPERTIES OF ION PLATED
NICKEL FILMS ON GLASS-CERAMIC SUBSTRATES

by

Mihir Mahendra Shah and J. M. Rigsbee
Department of Materials Science

A Report of the

MATERIALS ENGINEERING - MECHANICAL BEHAVIOR

College of Engineering, University of Illinois at Urbana-Champaign

January 1987

ABSTRACT

This investigation examines the relationship between the
structure, chemistry and resultant properties of nickel films
deposited onto cordierite glass-ceramic substrates via ion
plating (a plasma assisted physical vapor deposition technique)
using a combination of processing variables. Film adhesion,
evaluated using an expoxy bonded stub pull test, is used to
qualify the integrity of the metal/ceramic bond. A complete
range of structural and chemical microanalysis techniques,
including SEM, TEM, Auger microprobe, and SIMS, is employed to
characterize the nature of the film, substrate, and interfacial
region. Sputter cleaning prior to deposition has a pronounced
effect on adhesion, providing an excellent bond for films
deposited without an applied bias. Film morphology shows a
transition from columnar to equiaxed as the bias applied during
deposition is increased. Energetic particle bombardment from the
glow discharge can cause structural and chemical modifications of
the cordierite. Chemical mixing across the interface,
characteristic of ion plating, is confirmed. A processing window
is defined such that highly adherent nickel films can be
deposited on cordierite substrates via ion plating.

ACKNOWLEDGEMENT

iii

TABLE OF CONTENTS

I. INTRODUCTION

The research program described in this thesis involves ion plating of nickel films on cordierite glass-ceramic substrates. The objectives of the study are to determine the effects of the ion plating process parameters on the structure, chemistry and properties of the film, substrate and interface. These parameters are chosen such that an optimum processing window, based on the adhesive and morphological characteristics of the film, can be defined. Once the effects of each parameter are documented, mechanisms to explain the observations are formulated. Since it is often thought that the interfacial region between the film and substrate controls the properties of the system, a major effort to describe the nature of the interface is put forth. Through these investigations, a greater understanding of the fundamentals of the processes occurring in ion plating; e.g. energetic particle bombardment, sputtering, glow discharge characteristics, etc. is achieved. Ion plating was chosen as the deposition technique by virtue of its ability to produce adherent films. The nickel/cordierite system has its applications based in microelectronics packaging, where cordierite ($2MgO - 2Al_2O_3 - 5SiO_2$) is a possible replacement for alumina. The challenge of being able to deposit an adherent nickel film on a cordierite substrate is ideally suited to ion plating. The nickel/cordierite system provides a useful comparison to others being investigated in this laboratory, including copper/cordierite, copper/chromium/cordierite, and

1

titanium/cordierite.

The primary physical property analyzed in this program is film/substrate adhesion, as quantified by the Sebastian pull test. Adhesion is measured as a function of sputter cleaning and applied bias. Four point bend testing is used to evaluate the mechanical strength of the cordierite as a result of processing conditions. Microanalytical tools such as scanning and transmission electron microscopy, Auger electron spectroscopy, and secondary ion mass spectrometry are employed to correlate structural and chemical information to macroscopic properties.

Although this thesis covers a number of aspects of the program, it is by no means a final statement. Experiments are continuing in order to confirm and expand upon the results presented, and other types of analyses are being devised to provide answers to questions raised during the course of this investigation. Some of the questions being asked are the mechanisms for production of "altered layers" in the ceramic substrate, the mechanisms for adhesion promotion, and the effects of energetic particle bombardment on the cordierite surface.

2

II. BACKGROUND SURVEY

A. MICROELECTRONICS PACKAGING

The microelectronics industry is a major driving force behind materials science research today. Much of the work is involved with packaging technology, which involves developing new materials and processes in order to keep pace with the increasing complexity of computer chips. As the number of circuits per chip increases, providing power, interconnections, cooling, and housings becomes more difficult [1]. In many cases, the package may be the limiting factor in the performance of the system [2]. Novel and more complex packaging schemes, such as the IBM thermal conduction module [3] , have been developed to overcome this problem. This is, however, an ongoing program with new substrate/interconnect material systems and package designs being evaluated [4]. The prospects for the use of glass-ceramic substrates in this area are quite promising.

B. METAL/CERAMIC INTERFACES

One of the necessary qualifications for a ceramic substrate is the ability to metallize its surface. In order to achieve this end, an understanding of the interactions between metals and ceramics must be established. Of primary importance in the thin film area are the mechanisms for good metal/ceramic adhesion. Mattox has presented a number of factors which affect the adhesion of metal films [5]. Some of these, primarily the structure of the interfacial region, are applied to the

3

metallization of oxides in microelectronics [6]. The types of metallization described include depositing conductors on bulk oxides, metallizing thick oxide insulating films for interconnects, and metallization of thin, naturally occurring oxide layers on devices to produce good electrical contact. It is commonly accepted that in order to attain a consistent metal/ceramic bond, the metallic element must be able to react chemically with the ceramic, resulting in an interfacial zone. Formation of an interfacial zone via chemical reactions may be promoted by conducting the deposition at an elevated temperature. One must be aware that high temperatures may degrade substrate properties or those of pre-deposited films. A similar outcome can arise if the film material is soluble in the ceramic, producing an interfacial zone via diffusion. Unfortunately, in microelectronics packaging, a relatively noble film (e.g. Cu or Ni) is desired. This is due to thermal and electrical conductivity, oxidation resistance, and mechanical durability requirements. One method of achieving good adhesion in this case is by altering the chemistry of the ceramic surface. This may be done by implanting the surface with the desired ion [7], or by depositing a "bonding layer" between the substrate and the final film. Implantation of the surface can produce an alloyed or doped ceramic layer. This may result in a more reactive, metastable structure, with metal ions available to enhance bonding. It may also produce a new surface compound, e.g. a spinel, which allows the metallic film to adhere to it [8]. Deposition of a bonding layer is also done to form chemical compounds with the substrate,

4

film, or both. Again the possibility of forming a spinel with the ceramic is present, as well as the possibility of forming intermetallic compounds. Reactive metals such as chromium or titanium are often used for implantation or bonding layers because of their favorable free energy of formation of oxides.

As an alternative to chemically producing the required interfacial zone, energetic deposition techniques may be utilized. This may promote metal/ceramic adhesion through a number of effects. It is suggested [5] that the nucleation mode of the film may be altered, causing a change in the effective contact area, wich may be a factor in adhesion. Higher energy particles can also create a graded interface, with gradual transitions in chemical composition and lattice parameter across the interface, by enhancing diffusion. In addition to obtaining a sufficiently strong bond in the as deposited condition, one must also be aware of the subsequent processing sequences, such as chip reflowing, soldering, and brazing, which the metal/ceramic couple may undergo. Diffusion of elements across the interface, stress relief and precipitation all have the potential for degrading adhesion, particularly when the heat treatments are conducted in reducing atmospheres [6]. Diffusion and stress relief can cause a transformation from an adherent, metastable interface region to the equilibrium state, which may not provide adhesion. This may be accentuated if there is a high defect concentration in the interfacial region to act as a driving force for relaxation. Interfacial zones which have a concentration of metallic solutes greater than the equilibrium

5

solid solution as a result of energetic deposition or ion implantation may undergo precipitation upon heating. This could lead to brittle metallic phases at the interface. Reducing atmospheres, often used in chip attachment cycles, can be notorious for degrading the integrity of a metal/ceramic bond. Adhesion may be due to the presence of a spinel at the interface, which may decompose via a reduction reaction. Petzow et. al. [8] also presented a review on the nature of metal - ceramic interfaces. They contend that the quality of the bond is related to the microstructure of the interfacial region between the brittle ceramic and the more ductile metal. Microstructural evaluations, along with mechanical property analyses, are two primary methods used to investigate the metal/ceramic bond. Chemical reactivity is often quoted as a mechanism for bond strength, indicating that the free energy of oxide formation is the controlling factor, but more microstructural correlations are required. The authors employed fracture mechanics concepts to quantify the integrity of the metal/ceramic bond. Four point bend specimens, notched at the interface, were tested to determine fracture energy. Finite element analysis was then performed to describe the state of stress and calculate the fracture resistance of the bond. Microstructural examinations indicate the presence of a complex transition zone in many cases. One example provided by Petzow is the Cu - Al_2O_3 system, formed by a eutectic bonding process. Through the use of electron microscopy, a $CuAl_2O_4$ spinel layer has been detected at the Cu - Al_2O_3 interface. The metal, ceramic, and spinel all have certain

6

crystallographic relationships which can affect the bond strength. Combining the TEM data with fracture studies provides a useful correlation between interfacial microstructure and macroscopic behavior.

Arsentyeva and Ristic' [9] investigated the bond between nickel and aluminum oxide, cosintered at 1350 C. They reported that the Ni - Al_2O_3 system should be thermodynamically stable up to its melting point. At high temperatures, a $NiAl_2O_4$ spinel may be formed if the sample is heated in an oxygen atmosphere. Their experiments involved a nickel matrix with 40 volume percent oxide. They concluded that the bond is ionic-covalent and metallic, similar to an Ni_2Al_3 type. A strong bond is formed during cosintering when an Ni_2Al_3 film is formed between the nickel and the aluminum oxide.

Wlosinski [10] studied the Al_2O_3 - Cr and Al_2O_3 - Cu systems. Some of the properties deemed important are the oxide wettability of the metal, the possibility of chemical reactions and the solubility of the initial elements and reaction products. Various reactions in the Al_2O_3 - Cu system are described, with resulting interface compounds being formed. Other metals such as Ni and Fe are shown to have strong surface reactions with aluminum oxide.

In general, when bulk metal/ceramic composites are formed via high temperature bonding, chemical reactivity of the metallic species leading to the formation of an interface compound, often a spinel, seems to be the central theme.
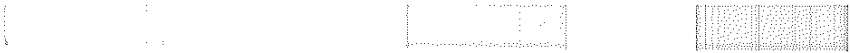
C. ADHESION

Adhesion between the film and the substrate is an important aspect of all coating and thin film technologies, particularly when applied to metal/ceramic systems as discussed in the previous section. Although it is often used to characterize the integrity of a film/substrate couple, as evidenced by the qualitative and quantitative evaluations reported later in this section, the term "adhesion" has varying connotations. An excellent review of the terminology of adhesion, as well as the factors which may influence adhesive behavior is given by Mittal in reference [11].

Mittal [11] says that the adhesion of the film to the substrate has a direct effect on the performance of the film/substrate couple. Adhesion measurements may be used to determine the result of changes in process parameters and define an optimum processing window. Information derived from adhesion tests spans the entire range of applications; from quality control, to the more scientific aspect of understanding the fundamental mechanisms of adhesion. Quality control can include using the scratch adhesion test to ensure that a given lot of coated parts will meet specifications for wear resistance. Adhesion tests of a fundamentally different type can be used to determine the energy required to remove an atom from a surface. Though both the industrial and the scientific methods generate adhesion data, they do not necessarily describe the same phenomena. Mittal suggests that as a result of the wide variety of physical properties measured by "adhesion" tests, further

elaboration is required when using the term "adhesion." The term "basic adhesion" is used to represent the interfacial bond strength, related to a summation of interatomic forces. Measurements of this type can be compared to bond strength calculations across an interface. Extreme care must be taken when conducting these experiments in order that only interatomic forces are measured, and not those related to practical adhesion. Mittal uses "practical adhesion" to indicate the separation of components at an interface or in an interfacial region. Practical adhesion may include the energy of deforming the film, the presence of sites for premature failure, and the intrinsic stress of the system. Practical adhesion can be a function of the film thickness, the method of applying the stress, and the failure mode. It is this practical adhesion which is generally measured and reported in the literature. Henceforth, the term "adhesion" will be taken to mean practical adhesion, unless specified as being otherwise. Adhesion depends on a number of factors, including the testing method and conditions, the failure locus and mode, in addition to the basic adhesion energy. There may or may not be a simple and direct relationship between practical and basic adhesion.

Mattox [12] describes adhesion as a macroscopic property dependent on the bonding across the interface, local stresses in the system, and the failure mode. Good adhesion is promoted by: 1) strong atom - atom bonding in the interfacial region (basic adhesion), 2) low local stress levels, 3) absence of easy deformation or fracture modes, and 4) no long term degradation

9

modes. As referenced in the previous section, Mattox proposes that the nuclei density and growth mode determine interfacial contact area, which affects adhesion. The nuclei density during deposition may be altered by ion bombardment, electric fields, gasseous environments, surface impurities and defects, and the particular deposition technique utilized.

Since adhesion depends on the nature of the interfacial region, Mattox has divided the types of interfaces into five categories. A mechanical interface is of the type found between a film and a rough surface, relying on mechanical interlocking with the rough surface for its strength. As an example, this study investigates the bond between a metal film and a rough, as received ceramic substrate. Abrupt, or monoloayer to monolayer, interfaces are those often found in semiconductor heterostructures [13]. They involve no diffusion and little chemical reaction, are confined to a 2 to 5 angstrom region, and are often the result of negligible solubility between materials. Compound interfaces involve regions of constant composition which extend over many lattice parameters. They result from chemical interactions, often in the form of an oxide or intermetallic. Interfaces of this type can be found when a reactive metal is deposited on an oxide ceramic [8]. Of concern with compound interfaces is the brittle nature of many of the compounds formed, as well as the stresses which can develop due to lattice mismatch [12]. The diffusion type of interface has gradual transitions in composition, lattice parameter and stresses across the region [12]. Although this type of interface is often associated with

high temperature processes, energetic techniques such as ion plating may yield the same result [14]. Interfaces formed via energetic processes are termed "pseudo-diffusion" by Mattox. This is used in conjunction with normally insoluble materials and/or nonequilibrium conditions. Note that an interface need not be limited to one classification, and that the guidelines for each category should only be taken as such.

Once the term "adhesion" has been defined, methods must be devised which can provide a measure of adhesive strength. A variety of such methods have been reported in the literature, ranging from simple to complex and qualitative to quantitative, and are summarized as follows. There are two primary categories for adhesion tests: tensile and scratch. Stoddart [15] tested adhesion of copper films on glass substrates using a tensile test. Brass rods were glued to the film using a fast setting cyanoacrylate adhesive (Eastman 910). A tensometer and load cell were used to measure the force, applied horizontally to the rod, necessary to remove the film. The stress distribution is assumed to be that of simple tension. A similar test apparatus is used by Kikuchi [16] to characterize silver films on glass. The test was referred to as the "topple test". Stainless steel cylindrical rods 6 mm by 50 mm were epoxy bonded to the films and cured for 24 hours. Horizontal force was applied to the rods via a spring and a motor. Adhesion strength was computed using equation (1).

$$\sigma = \frac{4hF_o}{\pi r^3} \qquad (1)$$

h and r are the rod height and radius, and F_o is the peeling force. The investigators also compared the topple test to a scratch test, using styli of varying hardness values. Pencil leads, sharpened to a 0.25 mm radius of curvature, were drawn across the film for 10 mm with an applied force of 120 gf. A comparison of the results from the two methods indicates that they are monotonically related. If the hardness of the scratch test stylus is kept constant, the relative peel length can be calibrated to adhesion strength. Scratch tests were also conducted by Perry [17]. A Rockwell "C" diamond indenter with a hemispherical tip of 200 micron radius was used. The stylus was drawn across the sample, with increasing force for each successive trace, until the coating was removed. This critical load is taken to be the value of coating adhesion. No quantitative analysis of the stress state is given; adhesion is simply reported as that load which caused coating removal. The failure mode was examined via optical and scanning electron microscopy. Determining the actual failure behavior during scratch testing is one of the difficulties with the test. The film behavior is often complex, and determining the actual adhesive force is not trivial. Adhesion failure is not necessarily associated with removal of the film. Detached film may remain in its original position without breaking. Films may be thinned to optical translucency, such that they may not be detected and thought to be detached from the substrate [18].

Jacobsson and Kruse [19] measured the adhesion of evaporated thin films on glass substrates via a direct pull method. In

12

their experimental arrangement, cylindrical steel blocks are cemented to either side of the film/substrate couple. Each block is connected to a bar, which is pulled in direct tension. As a requirement for validity of the experiment, the pulling force must be uniformly distributed over the area of the blocks and the failure must occur at the film/substrate interface. The adhesion strength is then given by equation (2).

$$\sigma = F / A \qquad (2)$$

F is the force to pull off the film and A is the area of the steel blocks. The investigators also examined the effects of various errors in the test. Misalignment of the rods will introduce a moment, which alters the state of stress. With typical values of misalignment, the error introduced is approximately 10 kp/cm^2, with adhesion strengths being 200 to 600 kp/cm^2. Non-uniformities in the thickness of the cement is also shown to introduce an error of 5% or less into the measured adhesion force.

Varchenya and Upit [20] examined adhesion of metal films on atomically clean quartz surfaces. They employed a direct pull technique using 3 mm diameter pins affixed to the film via an epoxy resin. To minimize bending moments, the pin height was equal to the diameter.

Mirtich [21] and Salem and Sequeda [22] performed adhesion experiments using a commercially available tensile adhesion tester. The Sebastian Coating Adherence Tester (made by Quad Group, Inc [23]) uses an epoxy coated, aluminum stub, which is bonded to the film by curing for one hour at 150 C. The stub is

13

then inserted into the instrument, which then pulls it in tension, giving a stress readout in Ksi. The failure strength of the epoxy is rated at approximately 45 to 62 MPa (6.5 to 9.0 Ksi), with the maximum load cell rating of 71 MPa (10.30 Ksi.) The major limitation of this technique is the strength of the epoxy, which often fails before the film is removed from the substrate. There is also a component of triaxial stress at the film/epoxy interface, which is not considered in the analysis. Also, if the epoxy does not flow correctly during curing, variations in the contact area (and the loaded area) of the film are introduced. The simplicity and relatively quantitative nature of the Sebastian test, along with the fact that is a widely used, commercially available unit, make it an attractive method for determining thin film adhesion.

Swaroop and Adler [24] tested the adhesion of copper ion plated onto steel substrates. A 90 degree bend test and a standard Scotch tape test were used. In the 90° bend case, the film/substrate couple was placed in a vise and bent to 90° in a continuous motion. The couple was then examined in an optical microscope for evidence of cracking. The Scotch tape test used Scotch Brand no. 810 tape, which supports an average pull strength of 2000 g/cm² (approx. 30 psi). No evidence of failure was found in any of the samples tested with the tape.

When choosing a method for evaluating film adhesion, a number of factors should be taken into account. The Scotch tape test is the easiest to perform, but is not useful for films with strong adhesion and is semi-quantitative at best. The direct

14

pull and Sebastian methods are also relatively easy to perform,
but can be limited by the strength of the bonding agent used.
Scratch tests are useful for highly adherent films, but data
interpretation is difficult, especially for ductile films. The
test method best suited to the situation should be determined by
considering the type of film/substrate combination and the type
of information desired.

D. THIN FILM TECHNOLOGY

Although thin films are becoming increasingly prominent
in materials research today, the technology has been present in
various forms for many years. An American Society for Metals
seminar in 1963 was devoted to the preparation, characterization
and properties of thin films.

Behrndt [25] begins by discussing various methods of
preparing thin films. One of the oldest techniques, and one
still in use, is electrodeposition. In simple terms; metallic
ions in solution migrate toward the cathode due to the applied
electric field. Many complexities are introduced, however, when
one considers the boundary layer between the cathode and the
electrolyte, as well as the composition of the electrolyte
itself. Although vapor deposition is thought of as a new
technology, it was first repoted by de Lodyguine in 1893 who
coated carbon filaments by heating them in H_2 and WCl_6 [26]. The
basic process of vapor deposition as described by Behrndt is the
reduction or decomposition of a volatile compound at the
substrate surface. This is actually chemical vapor deposition as

15

used today. Vapor deposition may be carried out in either an open tube, flowing system , or in an closed environment with convection currents transporting the gas. Sputtering from a cathode in a glow discharge was first reported by Grove in 1852 [27]. Note that in this 1963 symposium, Behrndt mentions that it is known that sputtering is caused by ionization of gas in the discharge, but that no quantitative theory has been established to match experimental observations. Much of the sputtering theory in use today was developed by Sigmund in the late sixties [28]. Planar cathode and anode configurations are described by Behrndt, with sputtering done in a simple glow discharge. Some attention is given to parameters affecting sputtering rate, as well as the technique of reactive sputtering.

Although evaporation appears to be the least complex of the deposition techniques discussed, it is the most recent. It was first conducted in vacuo by Pohl and Pringsheim in 1912 [29]. Two reasons why it began late were the difficulty in generating enough heat and the lack of suitable containers. Since gas incorporation into the film is a major source of impurities, the degree of vacuum is also an important requirement. Film formation characteristics are directly related to the state and properties of the substrate. The crystallographic state, surface roughness, and substrate temperature are all important parameters which can determine the morphology and orientation of the film. Factors such as the surface mobility will affect the nucleation of the film and determine whether or not, for example, the film will grow epitaxially.

Behrndt also discussed other factors which will only be mentioned briefly. Substrate preparation methods, including reduction of surface roughness, substrate heating, and ion bombardment are described. Methods for monitoring deposition rate, film thickness, and substrate temperature are reviewed. A section is devoted to the design and operation of evaporation systems. Finally, a comparison of the properties of films grown by the different techniques is presented.

Although Behrndt's paper was presented in 1963, it is very good in providing a historical perspective of the thin film industry. Many of the basic principles presented are still followed today. It is also a very thorough review of the literature of its time, complete with 232 references.

More current and in-depth reviews of thin film technology are given by Maissel and Glang [30] and Bunshah et. al. [31]. Because of the large amounts of information contained in these volumes, they will not be summarized here but will be referenced for specific topics in future sections. Suffice it to say that both volumes would serve as an ideal starting point for the reader who wishes to examine a particular aspect of thin films in greater detail.

Bunshah has also written a brief review of coatings for large scale applications [32]. Large scale is defined as either large production throughput or highly complex arrangements in small areas. The review begins by categorizing the types of coatings produced based on their primary function; i.e. optical, electrical or mechanical. The coating material may also be

described as simple or complex, as may the coating morphology. The basic deposition techniques employed can be broken down into physical vapor deposition (PVD), chemical vapor deposition (CVD), electrodeposition, electroless deposition, droplet deposition, bulk deposition, and surface modification. These classes can be further subdivided: PVD encompasses evaporation, sputtering, and ion plating. The coating apparatus may be batch type or continuous. The continuous, in-line coater is shown to have a number of advantages for industrial production including uniform product quality, minimal impurity pickup, and high throughput. A table, reproduced as table (1), describes the characteristics of the various deposition techniques. More complete discussions of the technologies for metallurgical, optical, and electrical applications are also included. As a conclusion, Bunshah discusses the economic considerations for various coating applications. This is a factor often neglected in a research environment and can pose some interesting questions.

As evidenced in this section, the field of thin films is quite broad. An understanding of the basic processes involved in the different deposition techniques is essential in determining which one is best suited to a given situation. This approach seems to be more practical than attempting to concentrate on any specific technique, especially with the advent of hybrid methods such as ion plating and biased sputtering. In an effort to achieve this end, each of the major processes in thin film deposition are discussed individually and in detail, primarily as related to ion plating, in subsequent sections.

18

	Evaporation	Ion plating	Sputtering	Chemical vapor deposition	Electro-deposition	Thermal spraying
Mechanism of production of depositing species	Thermal energy	Thermal energy	Momentum transfer	Chemical reaction	Deposition solution	From flames or plasmas
Deposition rate	Can be very high (up to 750 000 Å/min)	Can be very high (to 250 000 Å/min)	Low except for pure metals (e.g., Cu-10 000 Å/min)	Moderate (200-2 500 Å/min)	Low to high	Very high
Depositing species	Atoms and ions	Atoms and ions	Atoms and ions	Atoms	Ions	Droplets
Throwing power for: (a) Complex shaped object	Poor line-of-sight coverage except by gas scattering	Good, but nonuniform thickness distribution	Good, but nonuniform thickness distribution	Good	Good	No
(b) Into small blind holes	Poor	Poor	Poor	Limited	Limited	Very limited
Metal deposition	Yes	Yes	Yes	Yes	Yes, limited	Yes
Alloy deposition	Yes	Yes	Yes	Yes	Quite limited	Yes
Refractory compound deposition	Yes	Yes	Yes	Yes	Limited	Yes
Energy of deposit species	Low >0.1 to 0.5 eV	Can be high (1-100 eV)	Can be high (1-100 eV)	Can be high with plasma-aided CVD	Can be high	Can be high
Bombardment of substrate/deposit by inert gas ions	Not normally	Yes	Yes or no depending on geometry	Possible	No	Yes
Growth interface perturbation	Not normally	Yes	Yes	Yes (by rubbing)	No	No
Substrate heating (by external means)	Yes, normally	Yes or No	Not generally	Yes	No	Not normally

Table 1 - Characteristics of deposition techniques [32]

E. ION PLATING

1. General introduction

Ion plating is a hybrid plasma assisted physical vapor deposition technique, combining elements of vacuum evaporation and sputtering. It is the fundamental processes involved in ion plating with which much of the remainder of this background survey will be concerned. Detailed discussions of each of the major portions of the ion plating process will be followed by a review of experimental studies which have used ion plating. The following introduction to ion plating is taken largely from reviews on the subject by Mattox [14.33], Walley [34], and Teer [35].

Ion plating was first introduced into the literature in 1963 by Mattox [36]. A generic description for the term ion plating given by Mattox [33] is "a film deposition process in which the substrate surface and/or the depositing film is subjected to a flux of high energy particles sufficient to cause changes in the interfacial region or film properties compared to non bombarded deposition." Some of the benefits of ion plating are the ability to: "sputter clean" the surface; provide a high energy flux to the surface, achieving high temperature properties while maintaining low bulk temperatures; and to alter the surface and interfacial structure by creating defects, mixing the film and substrate material and influencing the nucleation and growth conditions [14]. Another advantage of ion plating is its good "throwing power", which is the ability to deposit a film on all

20

surfaces of the substrate [37]. This is unlike most other high
vacuum techniques, such as evaporation and sputtering, and is due
primarily to scattering events with the working gas atoms.

The ion plating process is conducted in a high vacuum
chamber, with base pressures in the 10^{-6} Torr range. Typical
systems are evacuated using a mechanical (rotary) - diffusion
pump combination, as shown in figure (1). Substrates are mounted
on a high voltage cathode, which is generally water cooled.
Source material is evaporated using either resistive heating,
electron beam evaporation, or a sputtering target. If an
electron beam system is employed, modifications in the basic
chamber design are necessary to maintain adequately high vacuum
(10^{-5} Torr) at the electron gun filament while plating is
occuring at approximately 10^{-2} Torr. This is accomplished by
using a two chamber design, introduced by Chambers and Carmichael
[38]. A Pressure of 1×10^{-2} to 5×10^{-2} Torr of working gas,
generally high purity argon, is maintained in the upper chamber
during plating in order to support the glow discharge. The glow
discharge is ignited by biasing the cathode negatively to 1.0 to
5.0 kilovolts, while the remainder of the apparatus is at ground.
The characteristics of this type of glow discharge will be
explained in greater detail in a future subsection. It is the
presence of this glow discharge at the substrate which
distinguishes ion plating from most other deposition techniques.
The discharge is established prior to deposition in order to
sputter clean the surface, and may be continued during deposition
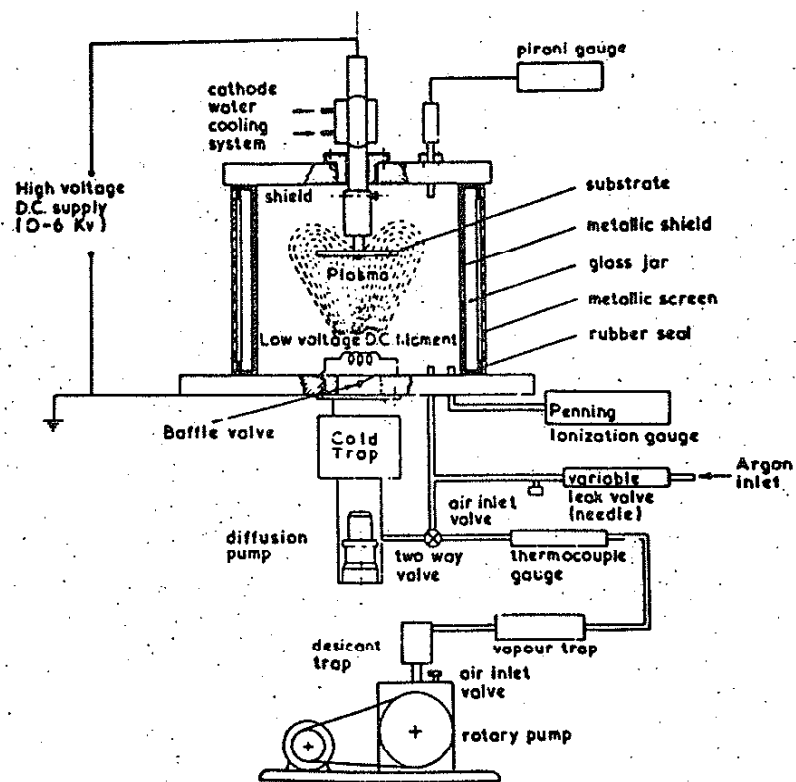to modify the film morphology.

21

Figure 1 - Schematic of a typical ion plating
system [35]

22

2. Glow discharges

Although ion plating has been described as a plasma assisted deposition technique, this is not strictly the case. The so called "plasma" is actually a glow discharge, which only approximates the conditions of an idealized plasma, which has a well-defined potential and density, and costituent particles in equilibrium motion [39].

A glow discharge can be established by applying a potential across two electrodes in a gas. The discharge will contain a number of different regions, some glowing and some dark, between the electrodes. These are illustrated schematically in figure (2), reproduced from reference [40]. Note that the diagram is for a normal glow, while ion plating involves an abnormal glow [34]. At low applied voltages, the discharge has constant voltage and current density, and is termed a "normal" glow discharge. When the power to the system is increased, the size of the region carrying cathode current increases until the entire cathode is used, initiating the "abnormal" regime. The general characteristics of the two discharge types are, however, similar. These two types of discharges are self-sustaining, meaning that the number of secondary electrons generated at the cathode is sufficient to maintain the discharge. In order for this to occur, the applied voltage must be greater than some minimum value (the breakdown voltage) or an auxilliary source of electrons is required to keep the glow from being extinguished. The simplest way to explain the properties of a glow discharge is to describe the events which occur in its various regions [30].
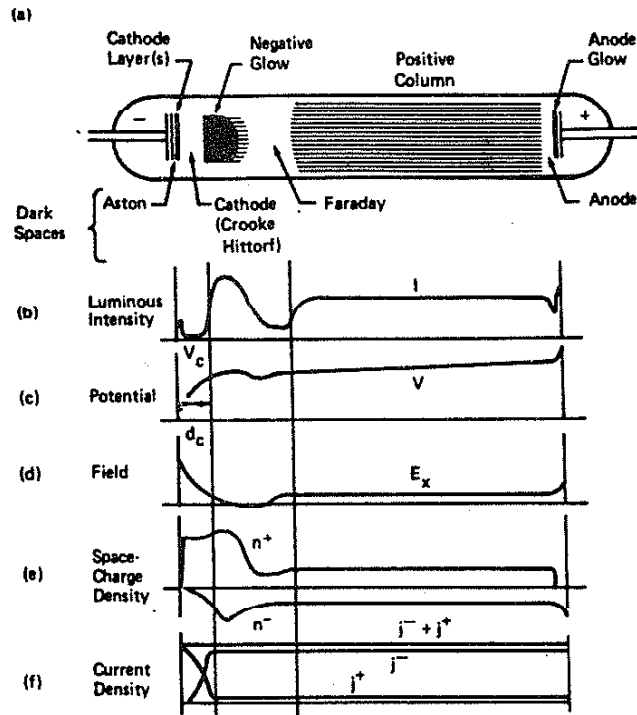
23

Figure 2 – Regions of a glow discharge [40]

The cathode dark space is of primary importance since it is the region adjacent to the substrate. It is also where positive ions accumulate in front of the cathode, producing a localized space charge and greatly increasing the electric field directly in front of the cathode. The extent of the dark space is approximately the distance travelled by an electron between ionizing collisions. Note that this distance is five to ten times larger than the mean free path, which takes into account other types of collisions. Electrons from the cathode experience the large positive electric field across the dark space and are rapidly accelerated toward the negative glow (an electrically neutral region), where they begin to produce ion - electron pairs. Because of the relatively neutral region produced, the ions in the negative glow move via diffusion until they reach the edge of the dark space and are accelerated to the cathode. The extent of the negative glow is determined by the range the electrons from the cathode have before they lose enough energy such that they no longer posess the ability to produce ions. This defines the far end of the negative glow, and is characterized by a build-up of electrons incapable of producing excitation, resulting in a dark region - the Faraday dark space. The positive column is the portion of the discharge which most resembles a true plasma, and is the most investigated. In most glow discharges used for deposition applications, however, the electrodes are closer together, and all that remain are the negative glow and the dark spaces adjacent to each electrode [39]. This does not affect the self-sustaining feature of the

25

glow, since this only depends on electron emission from the cathode and not on the anode position. In fact, a large portion of the negative glow can be extinguished before any effect on the electrical characteristics of the discharge is detected [30]. Charge transfer, the process in which an ion transfers its charge to a neutral atom, has an appreciable probability and must be considered. The high energy ion is now neutral, while the newly created ion has only thermal energy. According to Davis and Vanderslice [41], for a discharge of 600 V and 60 milliTorr most of the ions reach the cathode with negligible energy, and much of the cathode bombardment is due to energetic neutrals. A quantitative evaluation of the energy distributions of the particles is given in a later section. For a more detailed explanation of the processes occurring in a glow discharge, the reader is referred to the text by Chapman [39], which is written expressly for the non plasma physicist.

3. Ion plating processes

The following discussion of glow discharge processes will be restricted to those related to ion plating, and will be taken primarily from Walley [34]. In ion plating, the whole cathode is used by the glow discharge and there is sufficient current density to exhibit material transfer effects. The abnormal glow is operated in a self-sustaining condition, with a positive current/voltage characteristic. When designing ion plating cathodes, the extent of the cathode dark space is a prime concern. Grounded plates placed adjacent to the cathode will diminish the dark space, and if placed close enough will

26

extinguish the discharge. These ground shields are used to confine the glow to areas adjacent to the substrate. Since the anode configuration is not important in ion plating, it is generally taken to be the grounded vacuum chamber. The size of the dark space is a function of gas pressure; increasing as the pressure is reduced. This establishes the requirement that ion plating occur in a soft vacuum (10 to 50 milliTorr range). If the pressure is reduced far enough below this range, the dark space may extend to the anodes causing extinction of the discharge.

Figure (3) is a schematic of the events which occur during ion plating [14]. During sputter cleaning, no coating material is present in the vapor state. Gas atoms are ionized and accelerated across the dark space, during the course of which many become high energy neutrals via charge exchange. The high energy particles may be incorporated into the substrate or reflected, and may cause secondary electron emisssion or sputtering. The secondary particles created from the substrate may be redeposited on the substrate or on other parts of the chamber. When source (film material) atoms are introduced, the situation becomes increasingly complex. These atoms may be scattered, ionized or nucleated into fine particles (100 A). The ionized atoms will not feel the effect of the cathode until they reach the edge of the dark space. Of the film atoms/ions reaching the substrate, some may penetrate the surface, some are relected from it, and some remain to begin film formation. Also be aware that the processes described for sputter cleaning are
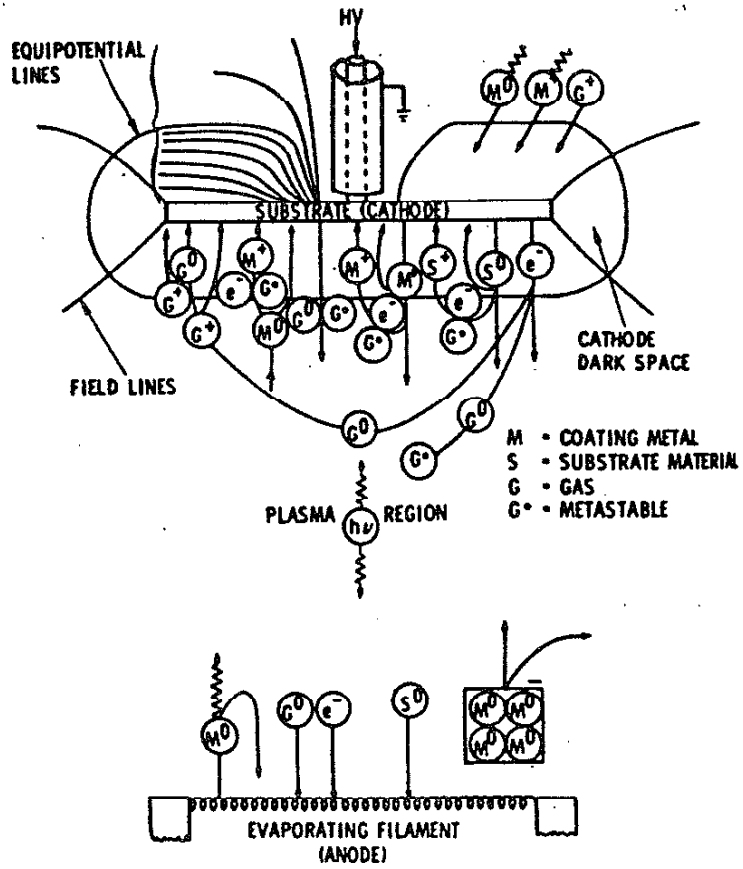
Figure 3 - Ion plating processes [14]

still active during deposition, if the glow is maintained. Although the types of events occurring are fairly well documented, there are still many questions unanswered. What is the ionization ratio for the film atoms and what is the distribution and average value of energy for particles impinging on the substrate?

A discussion of the ionization efficiency is given by Teer [35]. It is reported that estimates in the literature range from approximately 0.05 to 2.0 percent. By measuring the current collected at the cathode and comparing it to the number of incident particles, as calculated from the gas pressure, an ionization efficiency of 1.0 percent was arrived at by Teer. This approach, however, includes the contribution from ionized gas particles. Teer approximates the actual ionizatiion efficiency of film atoms at 0.1%. It then remains to be determined as to how this small fraction of high energy ions affects the deposition of a large number of low energy neutrals. In order to do this, the energy of the ions must be calculated. Davis and Vanderslice [41] have presented a theory of ion energy distribution, which has been experimentally confirmed. Using typical values for ion plating, the average energy of the ions is 10% of the maximum possible value, and the total energy deposited at the cathode by ions is approximately 10% of the energy dissipation in the system [35]. This energy, lost by the ions, is transferred to the neutrals. The maximum energy of a neutral is equal to the maximum energy of an ion, with 70% of the energy transferred to the neutrals reaching the cathode [42]. For the

29

equations used to obtain these results, please refer to appendix A. Under the conditions encountered in ion plating, deposition occurs via a small number of energetic ions and a much larger number of energetic neutrals. The average energies of the incident species are only 10% of the maximum possible, but are much higher than thermal energy, as is the case in most deposition techniques.

Rickards [43] used Monte Carlo simulation methods to determine ion and neutral energies in a glow discharge. The model uses typical glow discharge conditions; with the mean free path on the order of the dark space distance, a Boltzmann distribution of atom motion and an ion fraction of 10^{-4}. The potential near the cathode may be altered via a scaling exponent. Three types of energetic particles reach the cathode: ions that suffer no collisions and impact with the energy of the cathode voltage; ions produced by charge exchange collisions, whose energy is dependent on the position of their last collision; and energetic neutrals produced via charge exchange. Figure (4) is a plot of the fraction of ions which reach the cathode with maximum energy as a fuction of the dark space to mean free path ratio. Note that in the previous discussion, this ratio was taken to be 20. The Monte Carlo simulation results for determining the energy of the neutrals are shown in figure (5). Note the large drop in number as the L/λ ratio decreases. As a summary, Rickards indicates that for the case of $L/\lambda = 2$ and considering space charge effects, there will be twice as many neutrals as ions, with an average energy of 26%. Thus, more than 50% of the
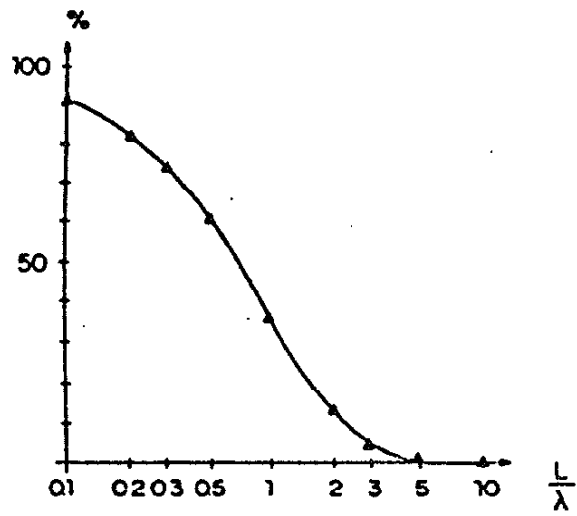
30

Figure 4 - Percentage of ions reaching the
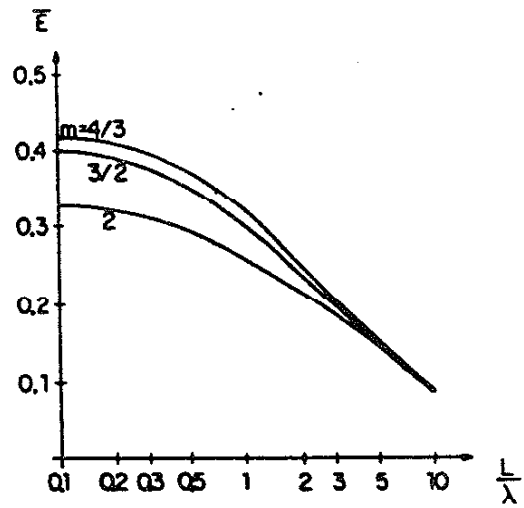cathode with full energy [43]

Figure 5 - Average energy of neutral atoms [43]

energy deposited at the cathode is attributed to neutrals.

Armour et al [44] monitored the energies of the incident flux to the cathode in an ultra-high vacuum ion plating system. The data was collected by allowing a fraction of the particles to pass through a pinhole in the cathode and be analyzed by energy and mass analyzers. Results indicated that the incident particles have energies significantly below the discharge voltage. For all cases studied, the peak in the energy distribution was at less than half the discharge voltage.

Although the applied bias is generally given as the parameter which relates to the energy of the incident flux, one should be aware that energy is more than just a function of applied bias. Three methods; calculation, simulation, and experiment have demonstrated that the energy of incident species is much less than the discharge voltage, and that energetic neutrals play a significant role in the ion plating process.

The glow discharge is one of the distinguishing features of the ion plating process, and also one of the common experimental variables. One of the areas of interest in ion plating research is to increase the intensity of the glow discharge. Saulnier et al [45] characterized the ion energies in a triode ion plating system, in which the third electrode was an anode ring biased up to +300 V. Increasing the discharge current while keeping the working pressure low decreases gas scattering and avoids difficulties associated with operating an electron gun at high pressures. This is accomplished by increasing the length of the electron trajectories. The ion energy distribution was measured

by collecting ions through a pinhole in the cathode. The discharge current increased as the ring voltage increased, due to trapping of secondary electrons in the positive potential well of the third electrode. This keeps them oscillating, increasing their path length, thus increasing their ionization probability. This effect is seen when evaporation is achieved via resistive heating, but is more pronounced when electron beams are used, due to to secondary electrons generated near the evaporation source. As shown in Figure (6), the ion energy distribution is shifted to higher values as the anode ring voltage increases. This is also due to the fact that the dark space is decreased with increasing anode voltage, resulting in less collisions.

The concept of triode ion plating was extended further by Matthews and Teer [46], who added a thermionic emmitter to the system in order to inject electrons independently from the evaporation source. A number of observations were made in their work. The use of a filament reduces current variations with pressure and also allows the discharge to be supported at lower pressures than in the normal diode configuration. Through the use of a negative filament along with a positively biased supplemental anode (see figure 7), ionization efficiencies of 3.0% can be attained, along with the ability to operate at pressures below 10^{-8} Torr.

4. Effects of ion bombardment

The effect of the glow discharge, central to ion plating, is to bombard the substrate/film with energetic particles. The results of this bombardment are what produce the properties
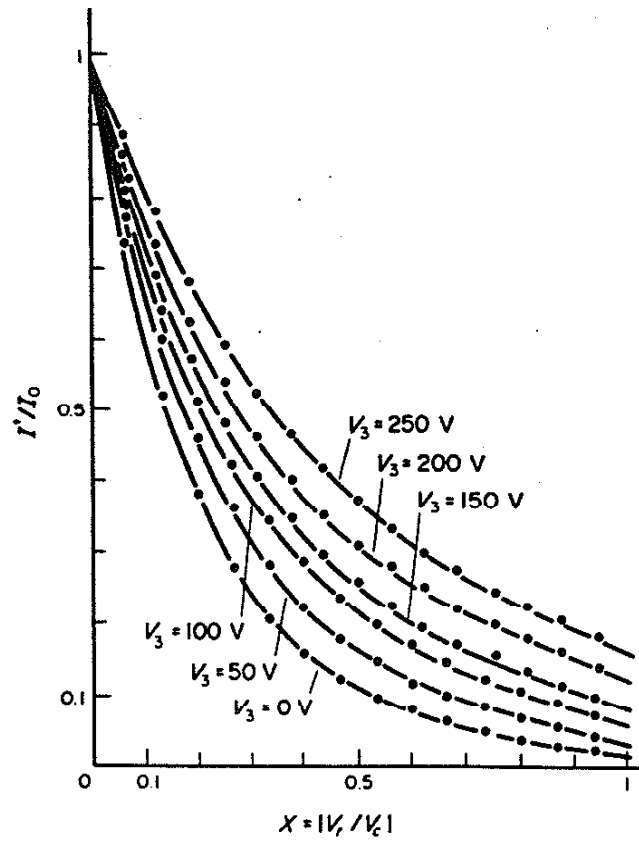
34

Figure 6 — Ion energy distribution for
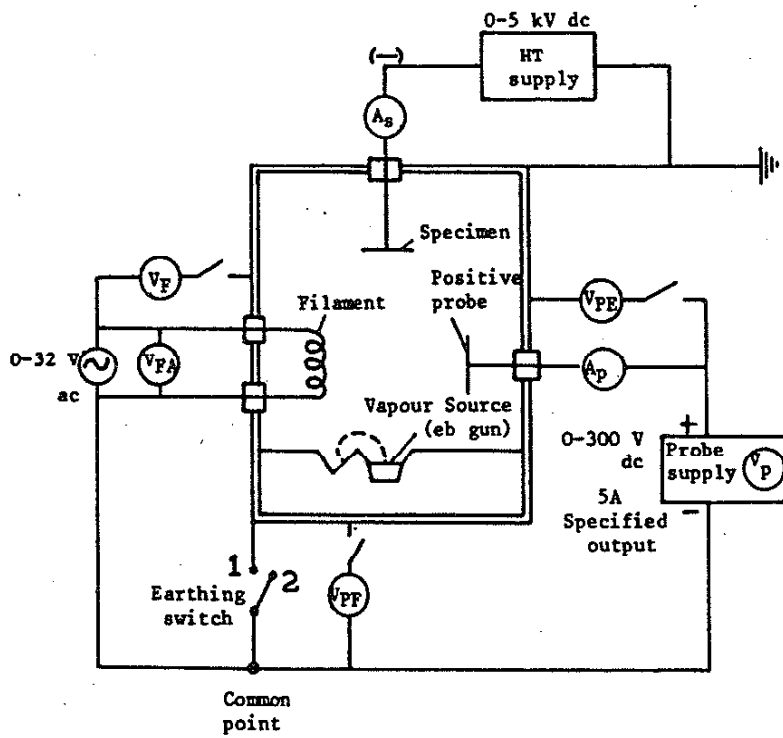various anode ring voltages [45]

Figure 7 - Thermionically assisted ion plating system [46]

characteristic of ion plating. Mattox [33] has addressed the
effects of ion bombardment in three regimes: prior to
deposition, during interface formation, and during film growth.
The primary effect of the discharge prior to deposition is
sputtering of the substrate surface, generally called "sputter
cleaning" in the case of ion plating. Sputtering, a complete
explanation of which follows in a subsequent section, causes
particles from the substrate surface to be ejected. It is via
this method that surface contaminants are removed, providing a
nearly atomically clean surface on which the film is grown.
Bombardment may also produce surface defects and alter the
surface morphology and crystallography. Since much of the energy
of the incident particles is dissipated as heat, there may be an
appreciable rise in surface temperature, causing problems with
thermally sensitive microstructures.

Interface formation at the onset of deposition can be of
great importance in determining the resultant properties of the
film/substrate couple, as described in an earlier section. Ion
bombardment during this stage can cause physical mixing of the
film and substrate elements via implantation, recoil mixing or
backscattering. Diffusion may also be enhanced due to the high
surface temperature and high defect concentration. All of these
processes favor the formation of diffusion or pseudo-diffusion
interfaces. The nucleation mode of the film is likely to be
determined by the particle bombardment. The bond strength
between the condensing film atoms and the substrate surface will
determine the mobility of the atoms. If the bond is weak,

37

mobility will be large and the atom will only nucleate at a high energy site or by colliding with other atoms, resulting in island growth. Conversely, a strong bond promotes the formation of a continuous monolayer. In general, an ion bombarded surface will provide more active nucleation sites by virtue of its topography and defect concentration.

Ion bombardment also has a large effect during growth of the film. It can affect morphology, crystallography and the accompanying physical properties. A preferential surface orientation or nucleation can lead to preferential growth and a cloumnar film morphology. This morphology, generally undesirable due to separation present between columns, may be avoided by depositing the film at elevated temperatures or by using the glow discharge as is shown in the following discussion.

The initial model for the morphology of evaporated coatings as a function of temperature was developed by Movchan and Demchishin [47]. Three zone structures, illustrated in figure (8), were detected. Below T_1, the structure is columnar with domed surface features. Between T_1 and T_2, the structure is still columnar, but has a smooth surface. Above T_2 the structure becomes equiaxed. An expansion of this model has been made by Thronton [48] to include the effect of argon pressure in a sputter deposition system (figure 9). Note that this still does not account for ion bombardment effects. Thornton [49] also added this effect into his model for the case of bias sputtering, with energies of a few hundred electron volts. The ability of ion bombardment to overcome the open boundaries resulting from
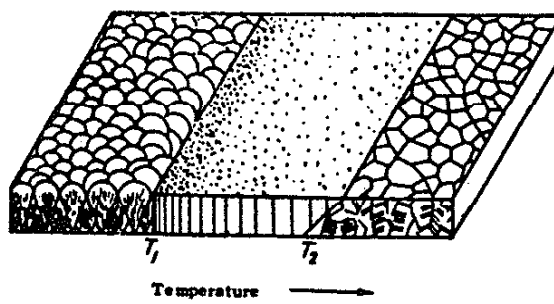
38

Figure 8 - Movchan - Demchishin zone
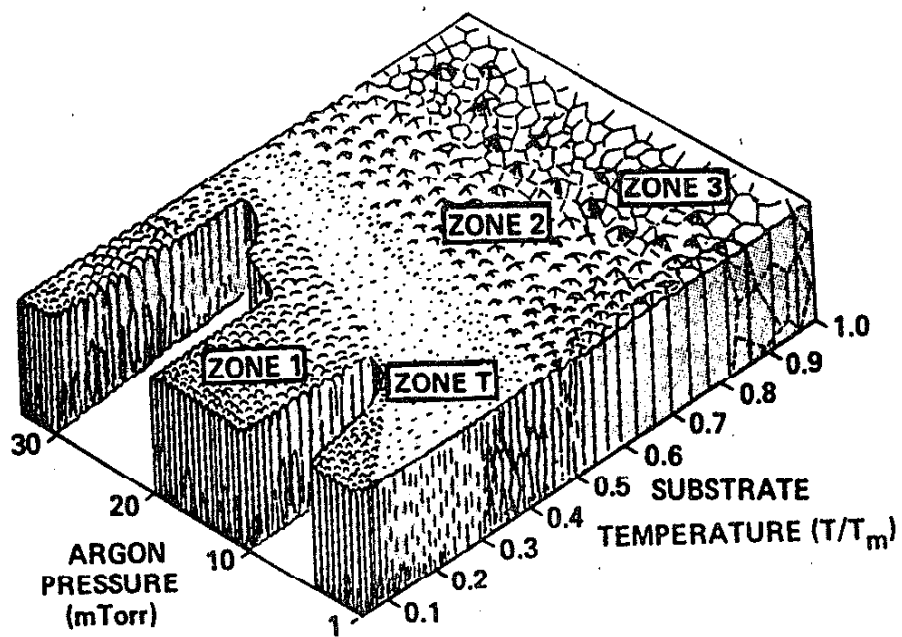structures [47]

Figure 9 - Thornton zone structures [48]

low temperature deposition was shown to be pressure dependent, with a larger effect at higher pressures. At the bias voltages employed in ion plating, which are up to an order of magnitude higher, the effect of ion bombardment is shown by investigators in this laboratory to have a pronounced effect on morphology similar to increasing the surface temperature. Thornton [49] has attributed the suppression of the columnar structure to redistribution of coating material by sputtering. The effect of the glow discharge is to produce films resembling a sputtered layer, rather than the porous structure obtained by evaporating in a soft vacuum without a discharge [34].

In addition to the mophological changes produced by ion bombardment, the intrinsic stress of the coating can be affected [33]. Evaporated films generally have a tensile stress, while sputter deposited coatings have a compressive one. Ion plated films may undergo a transition from tensile to compressive stress as the applied bias is increased; this is, however, still conjecture at this stage. Ion bombardment may also affect the adhesive properties of the film, as reported in previous sections.

5. Evaporation sources

In any physical vapor deposition technique, such as ion plating, coating atoms must be vaporized to generate the film. This may be done via evaporation or sputtering, but since ion plating generally uses evaporation this discussion will not include sputter deposition. The basic mechanisms of sputtering will be discussed in the next section because of their importance

41

in the glow discharge contribution. In evaporation, the material
is transformed into the vapor state when its vapor pressure
exceeds the pressure in the vacuum chamber. This has its basis in
classical thermodynamics, using the Claussius – Clapeyron
equation [50]. When the solid and vapor phases are in
equilibrium, their chemical potentials will be equal. The
general Claussius – Clapeyron equation (3)

$$\frac{dP}{dT} = \frac{Hg - Hs}{T(Vg - Vs)} \qquad (3)$$

is modified and rearranged for the particular case of a solid in
equilibrium with its vapor to give equation (4)

$$\ln p^* \; (Torr) = AT^{-1} + B + C\log T + DT + ET^{-2} \qquad (4)$$

where the coefficients are obtained from tabulated data and p* is
the equilibrium vapor pressure [30]. In practice, the solid is
simply heated until it begins to evaporate. By combining
classical thermodynamics with the kinetic theory of gases,
quantitative expressions for the evaporation rates can be
derived. The Hertz – Knudsen equation is used to calculate the
evaporation rate from a heated source. It is given in equation
(5) in the form most applicable to vapor deposition [48].

$$W = 3.5 \times 10^{-22} \alpha p^* (MT)^{-1/2} \qquad (5)$$

where W is the evaporation rate in atoms/cm²-sec, α is the
evaporation coefficient, p* is the vapor pressure in Torr, T is
the temperature in degrees Kelvin, and M is the molecular weight
in grams. The evaporation coefficient is an empirical parameter
ranging from zero to unity, and is highly dependent of the
cleanliness of the source surface. Atoms are emitted from the

42

surface with an average energy of 1.5kT, where k is the Boltzmann constant and T is the source temperature. They also follow a cosine law for spatial distribution of the emission flux [30]. Note that this distribution breaks down rapidly in ion plating due to the large amount of gas scattering present.

Experimentally, evaporation is performed by two principal methods: resistive heating and electron beam heating. Resistive heating is the original method, and is still in use in some ion plating systems. The material is placed in a refractory metal container, sometimes wrapped in tungsten wire (see figure 10). Large currents are passed through the container or wire, generating temperatures up to 2000 C. Some of the practical considerations of this technique are the limited amount of material which can be held at one time and the possibility of contamination from the crucible or support material. The more advanced method of evaporation is to use electron beams. The original electron beam gun involved a thermionic emission filament maintained at a high negative potential placed near the source, which is kept at ground. The electrons are thus accelerated into the source, where they dissipate their energy as heat. This type of gun has been replaced by electron guns with self - contained anodes and magnetic deflection systems. The source material is placed in a water cooled crucible, which is swept by the electron beam. Because of the problems associated with operating an electron gun in a relatively low vacuum, as described previously, some modifications in the standard assembly are made for ion plating systems. The filament is maintained in

43

RESISTANCE HEATED WIRE

a

METAL FOIL SOURCE

b

RESISTANCE HEATED CRUCIBLE

c

SUBLIMATION SOURCE

CHROMIUM
ROD

RADIATION
SHIELDS

HEATER

d

RF HEATED CRUCIBLE

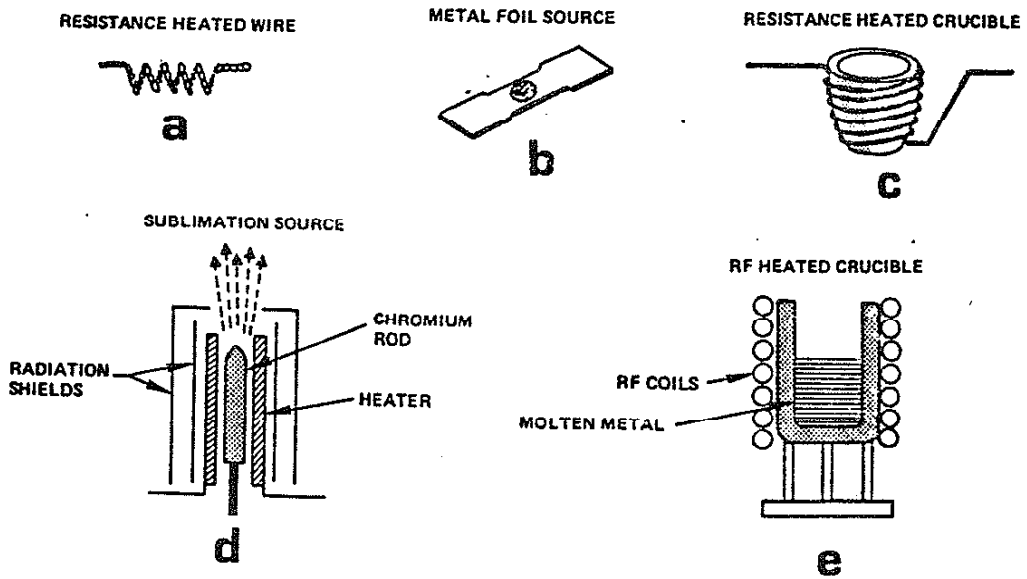RF COILS

MOLTEN METAL

e

Figure 10 - Resistive heating sources [48]

a chamber differentially pumped from the chamber which houses the glow, with the beam passing through a small hole separating the chambers and bent 270 degrees to contact the source surface. Electron beam sources have the advantages of being able to evaporate refractory metals, avoid contamination by only melting a local area of the source, and being able to hold a large amount of material.

6. Sputtering

Although ion plating systems generally do not use sputtering sources to generate the deposition flux, sputtering of the substrate and growing film occurs as a result of the glow discharge. A simplified review of the basic mechanisms of sputtering is given in reference [48]. In the sputtering process, a surface atom is ejected due to the transfer of momentum when the surface is bombarded by energetic particles. In ion plating, the negatively biased substrate is bombarded by energetic ions and neutrals from the glow discharge. The fundamental process in physical sputtering (as opposed to chemical sputtering, where volatile species are created) is the atomic collision. This is modelled as a binary, hard sphere elastic collision in most sputtering theories. A schematic of the events which occur and the energy transfer process are shown in figures (11) and (12) respectively. By virtue of the model, the most efficient momentum transfer occurs when both the incident and target particles have similar masses; thus argon is most often used as the working gas for the glow discharge. Since a single collision can not cause a target atom to be ejected,
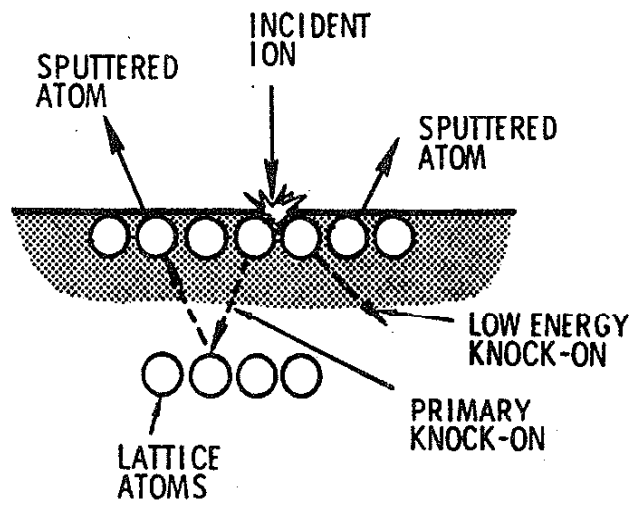
45

Figure 11 – Sputtering events [48]

INCIDENT
ION

M_i V_i

$-V_i' = \left(\dfrac{M_i - M_t}{M_i + M_t}\right)V_i$

M_t $V_t = 0$

TARGET
ATOM

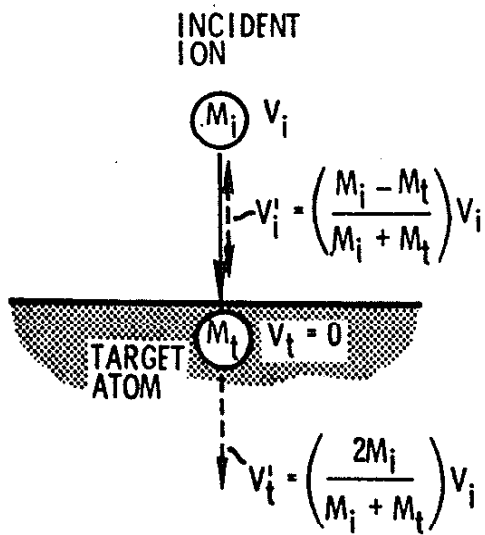$V_t' = \left(\dfrac{2M_i}{M_i + M_t}\right)V_i$

Figure 12 – Energy transfer during sputtering [48]

based on geometrical considerations, sputtering is a result of multiple collisional processes. With incident energies in the range of a few hundred electron volts, as is the case for a glow discharge, the major contribution to sputtering comes from low energy knock-ons (figure 11). Depending on the situation, the collisional cascades present in sputtering can be categorized in three groups: the single knock-on regime where atoms may be sputtered but lack sufficient energy to produce recoil cascades; the linear cascade regime in which recoil cascades are generated but only a fraction of the atoms in the cascade volume are in motion; and the spike regime in which most of the atoms in the cascade volume are set in motion by recoil atoms. In ion plating, only the single knock-on and linear cascade regimes are important. Theories have also been developed to describe the number of target atoms ejected per incident particle, known as the "sputtering yield." Although sputtering yields are often determined experimentally, Sigmund's linear cascade theory correlates well with experiment and is widely used [28]. The expression for sputtering yield, S, is given in equation (6), where K is a constant ranging from 0.1 to 0.3, M_i and M_t are the incident and target atom masses, E is the incident particle energy. U_o is the binding energy of the target atoms and $\propto (Mt/Mi)$ is a tabulated function.

$$S = K \; \frac{M_i M_t}{(M_i + M_t)^2} \; \frac{E}{U_o} \propto (M_t/M_i) \qquad (6)$$

The sputtering yield of most metals ranges between 0.5 and 5.0 and is not a function of temperature. Quantitative expressions

48

are most valuable in sputter deposition, but are also useful in ion plating to compare the evaporated flux of film atoms to the amount being sputtered away. The sputtering rate relative to the deposition rate can have a significant effect of the coating morphology [33].

7. Experimental review

As a conclusion to the background survey section of this thesis, three investigations of ion plated films are reviewed. Enomoto and Matsubara [51] analyzed the structure and properties of copper films ion plated onto tungsten substrates. An electron beam evaporation source was used, and additional plasma ionization was provided via three thermionic emitters. By varying the applied bias and ionization enhancement, the coating morphology was altered. At low bias and no enhancement a columnar morphology with porosity between columns was observed via SEM. When enhancement was used, a dense equiaxed morphology was obtained. In some cases, under conditions of low bias, a layered structure consisting of an initial dense layer followed by a porous columnar layer was present. A similar type of structure has also been detected as part of this investigation. Friction and wear properties were shown to be a function of film morphology, with the equiaxed structure being optimal.

Minni and Sundquist [52] investigated aluminum bronze coatings deposited on mild steel substrates via ion plating. The coating material was resistively heated, and the discharge current was controlled by an auxilliary filament. The coatings showed a compositionally layered structure as a result of the

different vapor pressures of the alloying elements and the batch fed nature of the evaporation source. The chemically mixed interface region, measured using Auger electron spectroscopy depth profiling, was shown to broaden with increased cathode current density. The morphology also changed from columnar to equiaxed with increased current density.

Pulker et al [53] examined the structure of reactively ion plated oxide films on glass substrates. All the crystalline films analyzed were fine grained and polycrystalline in nature. The ion plated films had a dense microstructure, while evaporated ones were less dense, with a columnar morphology. The presence of compressive stress in the ion plated films was confirmed via bending experiments. This is attributed to the impingement of high energy particles during deposition. The authors conclude that reactive ion plating is a viable technique for producing high quality oxide films.

III. EXPERIMENTAL PROCEDURE

A. MATERIALS DESCRIPTION

The source material used to grow the films in this study was 99.9% pure nickel, obtained from Aesar, Inc. The nickel was in the form of spheres, ranging from approximately 5 mm to 15 mm in diameter. Initial attempts to vacuum arc melt the spheres prior to placing them in the electron beam crucible proved ineffective due to contamination and gas entrapment. Subsequently, the spheres were placed directly into the crucibles and consolidated in situ.

The substrate material was a cordierite glass – ceramic, with the approximate composition ratios of $2MgO - 2Al_2O_3 - 5SiO_2$. (see figure 13,[54]) Substrates were in the form of square tiles, with thicknesses of a few millimeters. The squares were either 36 or 48 mm on edge. In the as received condition, the surface roughness was 250 nm. The substrates were mechanically polished, with progressively decreasing sizes of diamond paste, to a surface roughness of 25 nm before coating.

B. ION PLATING SYSTEM

All of the films in this study were grown using the ion plating facility of the Construction Engineering Research Laboratory (CERL), operated by the United States Army Corps of Engineers and located in Champaign, Illinois. The plating system was built by Torr Vacuum, Inc.. The vacuum chamber of the system is a split chamber design, allowing easy access to the interior.
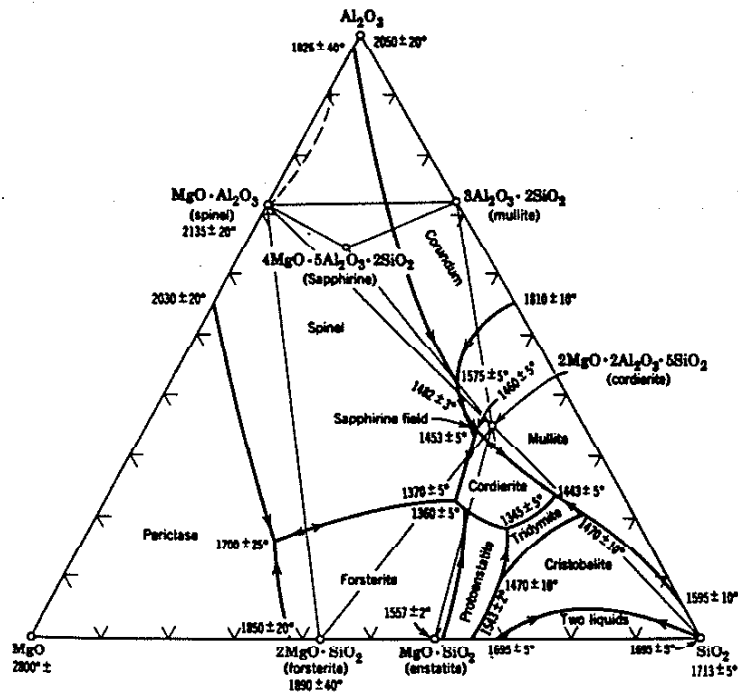
Fig. 7.30. The ternary system MgO-Al₂O₃-SiO₂. From M. L. Keith and J. F. Schairer, *J. Geol.*, **60**, 182 (1952). Regions of solid solution are not shown: see Figs. 4.3 and 7.13.

Figure 13 - MgO - Al₂O₃ - SiO₂ phase diagram [54]

A power driven hoist is used to raise the upper chamber, which
may then be pivoted about the hoist axis as desired. The chamber
is cylindrical, with a diameter of 0.66 m. The source to cathode
distance is 0.30 m. All vacuum seals in the system, with the
exception of the conflat feedthroughs, are made via rubber
O-rings. The entire chamber is water cooled to avoid damage to
the seals. Both the upper and lower halves of the chamber have a
variety of ports to accomodate the accessories to the system. In
addition, the upper chamber has two 0.115 m diameter viewports to
allow observation of the chamber interior during an experiment.
Disposable glass inserts are fitted to the inside of the
viewports to minimize down time between runs due to coating of
the windows. A "baffle plate" is placed in the lower chamber to
isolate the electron gun assemblies from the soft vacuum in the
upper chamber. The cathode, which acts as the substrate holder,
is a machined cylindrical stainless steel disc with a pattern of
tapped holes in its lower face. The holder, which is water
cooled. is welded to a pipe which passes through the chamber lid.
Electrical isolation and vacuum integrity are achieved via a
machined block of teflon, designed similar to a conflat.

The pumping system for the ion plater consists of 0.254 m
and 0.152 m diffusion pumps working in parallel, backed by a
single rotary pump. The pumping sequence is automated, with
manual override capabilities. Liquid nitrogen is supplied to the
diffusion pumps to achieve maximum pumping efficiency.
Evaporation is conducted via two electron beam evaporation
sources, allowing alloy and multilayer films to be deposited

without breaking vacuum. For single component films, it provides redundancy should one source fail during deposition. Each gun assembly consists of a water cooled copper crucible, a thermionic emission filament, and a magnetic beam deflection system. They are powered by an Airco Temescal CV14 power supply, generally operated at 10 kilovolts and 0.2 to 0.5 Amperes per gun. Retractable shutters are placed over each crucible to prevent unwanted deposition during source warm-up. Power to the cathode, needed to support the glow discharge, is provided by a Sloan model 7 high voltage power supply capable of delivering 7.5 kilovolts and 0.75 amps d.c.. The system is equipped with interlocks to prevent contact with any of the high voltage components while in operation. Gases are delivered to the system through stainless steel lines, with the flow rates adjustable via mass flow controllers. High purity argon, oxygen, nitrogen and acetylene can be admitted to the chamber, with each gas having its own calibrated mass flow controller capable of flow rates up to 50 sccm. In addition, laboratory grade nitrogen is delivered to the chamber through a vent valve in order to return the system to atmospheric pressure.

Accessories to the system include a residual gas analyzer (RGA) , Inficon model 1000 , used to monitor gas content and composition prior to and during deposition. It is primarily used during reactive ion plating of titanium nitride, conducted by other investigators in this laboratory. The RGA is also equipped with leak checking capabilities, allowing leaks to be detected by locally injecting helium around the seal in question and

54

monitoring the helium signal on the RGA. A triode enhancement system may also be connected to the system, if desired. It consists of a copper ring, mounted concentrically with the cathode, and biased positively. Four Hewlett - Packard d.c. power supplies, each rated at 60 V and 5 A, are used to drive the anode, with common operating voltages being 50 to 100 volts. Other options being evaluated or installed include a radio frequency high voltage power supply to allow more efficient sputter cleaning of insulating substrates; a quartz crystal thickness monitor to provide in situ deposition rate information; an upgraded pressure monitoring system; a titanium getter furnace to further purify the incoming gas supplies; and an optical spectroscopy system to characterize the constituents of the plasma during deposition. A complete schematic of the ion plating system is shown in figure (14).

C. DEPOSITION PROCEDURE

Prior to each set of deposition runs, the interior of the vacuum chamber is covered with clean aluminum foil. This allows for minimal down time when changing material systems, as the old aluminum foil may be removed and discarded. Either a pre-melted charge or fresh nickel pellets are placed in one or both of the electron beam gun crucibles, and a dummy deposition is conducted. This serves two purposes: to consolidate the charge without having to worry about splattering from an unstable charge ruining a substrate; and to coat all exposed aluminum foil and fixtures with nickel to effectively negate the possibility of
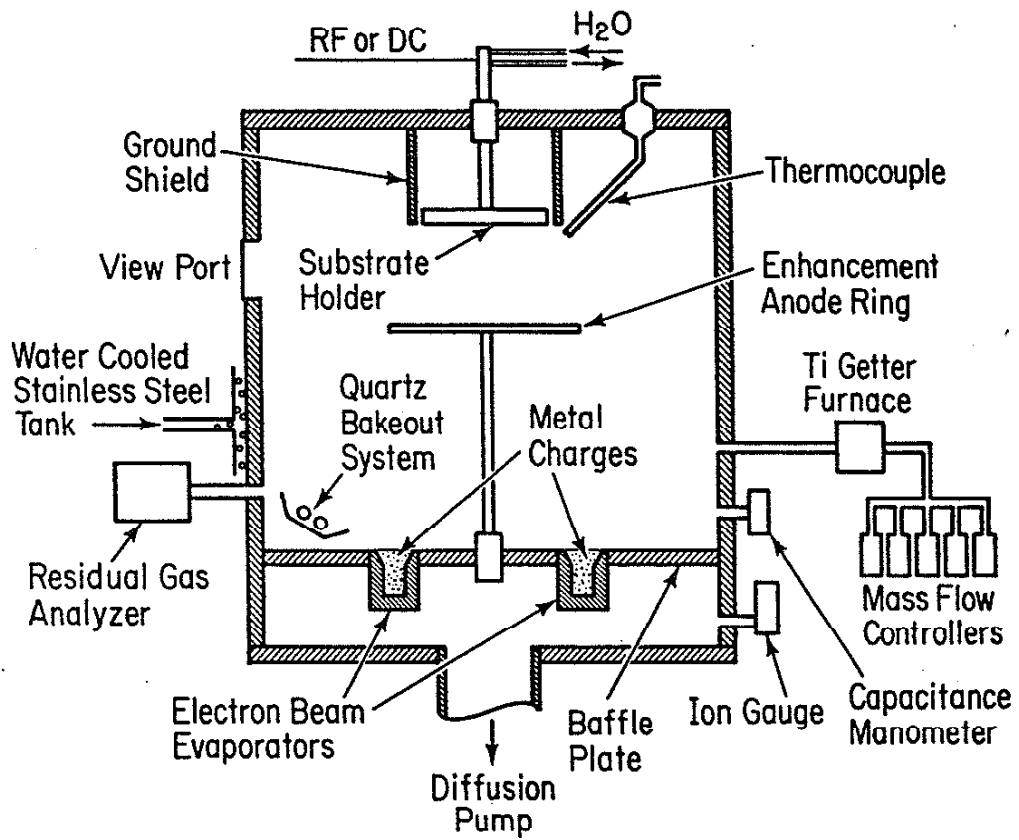
Figure 14 - Schematic of CERL ion plating system

contamination due to backsputtering. The chamber is then vented, after being allowed to cool to approximately 50 C, and substrates are mounted onto the cathode using nickel plated hardware. Overlapping pieces of silicon wafer were also placed on the cathode to be used as a thickness monitor. Precautions such as using gloves and tweezers were taken to preserve cleanliness. Once the source and substrates are loaded into the system, the chamber is evacuated to its base pressure, i.e. with no working gas present. When the base pressure is attained, the desired flow rate of gas is introduced and the system is allowed to equilibrate. If sputter cleaning is desired, the bias to the cathode is applied, igniting the glow discharge. A few minutes prior to the desired start of evaporation, the electron beam is turned on. This allows the source to be slowly heated to the vaporization temperature and maintained at a point where any small amount of evaporation occurring would be blocked by the shutter. When deposition is desired, the shutter is opened, the power to the electron beam is increased, and evaporation commences quickly since the source has already been preheated. Upon completion of the deposition, the gun power is turned off, the discharge is extinguished, and the chamber is allowed to cool. When the chamber has reached approximately 30 C, it is vented and the specimens removed. The chamber is exposed to the atmosphere as little as possible between runs to minimize the adsorption of water molecules to the chamber walls.

IV. ANALYTICAL PROCEDURE

A. ADHESION

Adhesion, as employed in this study, is used to characterize the macroscopic film/substrate bonding force. It is generally the first test performed on a set of films, due to its importance in defining a processing window and its relative simplicity. Adhesion tests are conducted using a Sebastian adherence tester [23]. This is a tensile test, in which an epoxy coated aluminum stub is bonded to the film via a cure cycle of 1 hour at 150 °C, with pressure being applied to the stub. The stub is then inserted into a receptacle in the unit, which applies a tensile load to it. When failure occurs, the load is removed and the stress readout is displayed. Both the failure load and locus, i.e. epoxy or film/substrate interface, are recorded. In addition to measuring the adhesive strength in the as plated condition, samples were also analyzed after being subjected to a thermal cycle treatment. This involved sealing the samples in an evacuated glass tube, backfilled with a partial pressure of either pure argon or an argon 10% hydrogen mixture, and heating them to a maximum temperature of 400 °C for a total cycle time of approximately 45 minutes. Although actual numbers are computed as adhesion results, one must be careful to treat these only in a relative sense. Variations in percentage of the area failing at a given interface can drastically affect the results. The location of the failure may be more meaningful than the failure load.

B. ELECTRON MICROSCOPY

Both scanning and transmission electron microscopy were utilized in this study, with TEM being a major focus of the analytical procedure. The SEM micrographs were taken using an ISI DS-130 dual stage scanning electron microscope, located in the University of Illinois Center for Electron Microscopy. SEM photographs were taken of fracture surfaces of the coating and substrate obtained while sectioning the coated substrates. This provided a reasonably accurate representation of the film morphology, due to the brittle nature of the substrate. Both film morphology and thickness were analyzed via the SEM, but limitations arose due to the small film thicknesses. As a result of this, the emphasis was placed on transmission electron microscopy, with its inherently better resolution. One of the drawbacks of TEM, however, is the difficulty in specimen preparation. This problem is compounded in this investigation by the need to produce a thin cross section of the interface between two very dissimilar materials. As part of the research in this laboratory, a method of preparing cross section TEM specimens, allowing direct observation of the film, substrate and interfacial structure and chemistry was developed. It is based on sandwiching two coated substrates together, with the film sides in contact, and placing them in a 3 mm diameter tube. The assembly is stabilized with epoxy, and discs may be sectioned using a low speed diamond saw and thinned via dimpling and ion milling. A complete, illustrated guide to this procedure is

59

provided in appendix B. The TEM micrographs were taken using Philips 400 and 430 analytical electron microscopes and much of the microchemical data was obtained via a Vacuum Generators HB-5 STEM, all located in the Center for Microanalysis of Materials at the University of Illinois. Bright field and dark field imaging, selected area diffraction and energy dispersive analysis of x-rays (EDAX) techniques were utilized.

C. SURFACE CHEMISTRY

Surface chemical analysis was conducted using Auger electron spectroscopy (AES) and secondary ion mass spectrometry (SIMS). The two techniques provided information on the film cleanliness along with composition vs depth profiles. The use of AES to determine the width of the chemically mixed interfacial region was not sucessful. No variations were detected as a function of processing conditions, due to interfacial roughness and instrumentally induced mixing as a result of the sputtering required to profile into the sample. A "reverse profile" technique was developed in conjunction with the SIMS analysis to examine the interface. For the cases in which the film was completely removed from the substrate during adhesion testing, the adhesion stub, now with film adhered to it, was placed in the SIMS. The exposed film surface is now the one which was originally in contact with the substrate. This allows the film adjacent to the interface to be analyzed without having to profile through the bulk film. Profiles can then be made into the bulk film a short distance until the composition reaches its

bulk values. This technique is, however, limited to films with poor adhesive strength.

D. SURFACE TOPOGRAPHY

The topography of the substrates, as well as the thickness of the deposited films, was analyzed using a Tencor Instruments alpha - step profilometer. This method uses a diamond stylus which is moved along the surface for a 3 mm trace. The stylus is mounted on a pivot, allowing it to move up or down following the contour of the surface. The background roughness of the substrates before and after polishing is determined in order to evaluate the effectiveness of the polishing procedure. Film thicknesses may also be determined via this technique. Two requirements which must be satisfied are a substrate surface which has a background roughness value much smaller than the thickness of the coating, and a sharp step between a coated and uncoated region. To acheive this, overlapping pieces of silicon were used. A trace is then made going either from uncoated to coated silicon, or vice versa. This method of thickness determination was used as a cross check to the electron microscopy measurements.

E. FOUR POINT BEND

A four point bend test was used to evaluate the mechanical strength of the cordierite substrates as a function of processing history. Samples were sectioned into bars 5 mm x 36 mm x 3 mm and tested in the as received or processed condition. The bars

were placed into the four point bend fixture with the processed side down (in tension) and loaded until failure. The failure load is then converted to an average breaking stress. Four point bending was used because of the relatively uniform applied stress distribution between the inner spans; and the processed side was placed in tension since this is the manner by which most ceramic samples fail.

VI. RESULTS

A. INTRODUCTION

The results obtained in this investigation are presented in the following subsections. Analysis of the surface topography of the substrates is presented first, followed by an evaluation of the mechanical properties of the film/substrate couples. Coating morphology, as evidenced by SEM, is compared as a function of process parameters. Information concerning the structure and chemistry of the film, substrate and interface obtained in the TEM is presented. Lastly, surface chemical data and concentration vs depth profiles taken in the Auger microprobe and SIMS are given.

B. SURFACE TOPOGRAPHY

Figures (15-17) show alpha-step surface profiles of an as received, polished, and sputter cleaned polished cordierite substrates, respectively. All traces are three millimeters in length, with the vertical scales as indicated. The background surface roughness is seen to be reduced by an order of magnitude, from approximately 250 nm to 25 nm, after polishing. Some of the larger defects such as pores and pits persist, due to the limited depth of the polish. Sputter cleaning did not alter the overall topography of the surface, although some of the upward deviations from background smoothness (fine hillocks) are diminished.
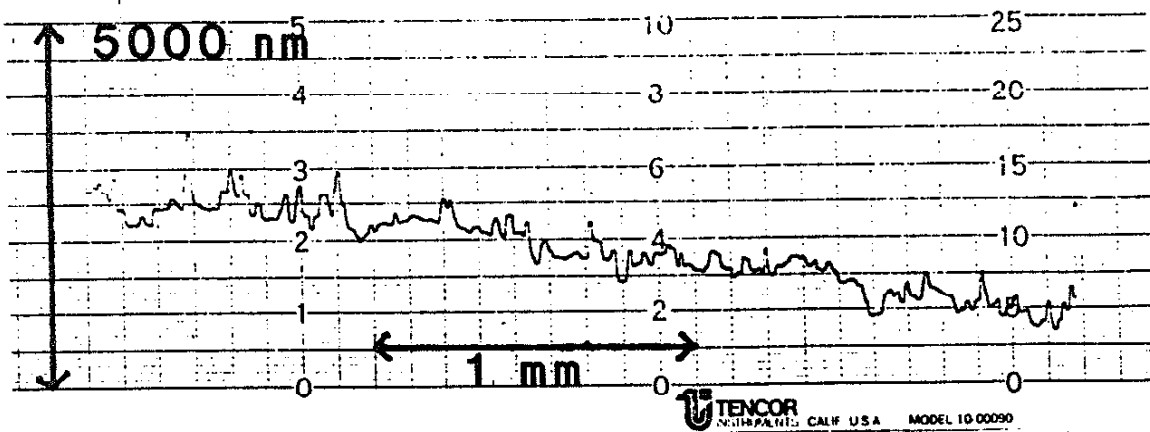
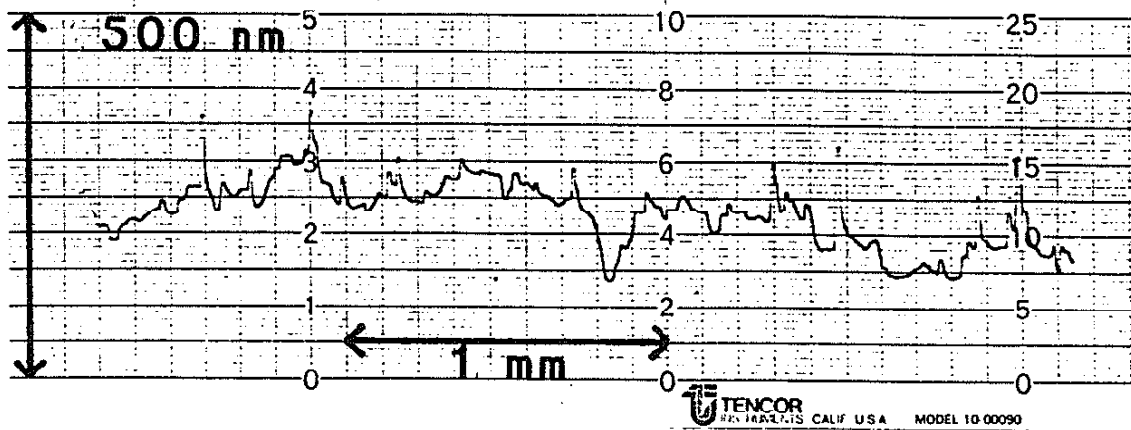63

Figure 15 - Surface profile of as received cordierite
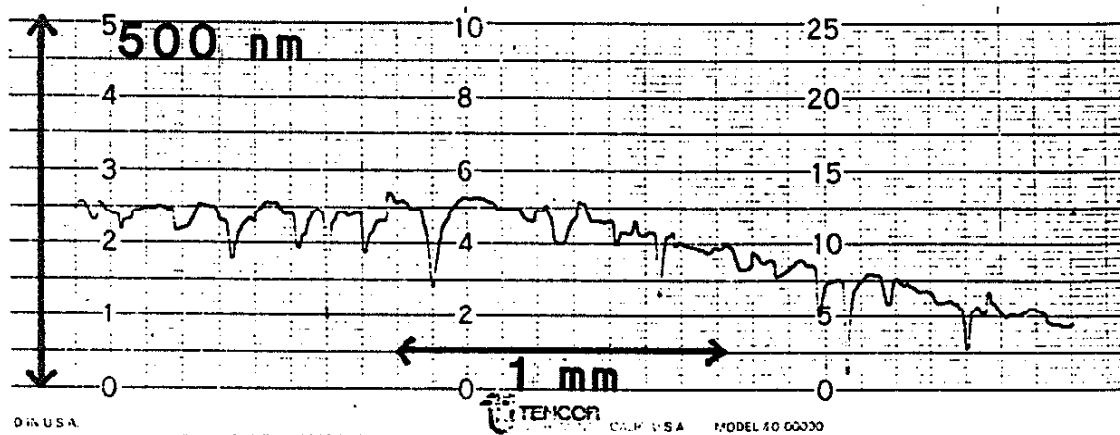
Figure 16 - Surface profile of polished cordierite

Figure 17 – Surface profile of sputter
cleaned, polished cordierite

C. SPECIMEN PARAMETERS

The ion plating process parameters used as variables in this study are shown in table (2) for all the coatings produced. Initially, applied bias was used as the independent variable, with series II substrates not sputter cleaned prior to deposition and series III substrates subjected to a 2.0 kV cleaning operation for 10 minutes. Because of the drastic differences in adhesive behavior between the two series, both applied bias and the use of sputter cleaning were varied independently in producing series IV specimens. All other operating conditions were maintained as constant as possible throughout the experimental matrix, with the typical values given in table (3).

D. COATING THICKNESS

Although evaporation time was kept constant for all films deposited, large variations in coating thicknesses are observed. Perhaps most significant are the discrepancies among the three techniques by which thickness measurements were obtained: alpha-step profilometry, SEM and TEM. Alpha-step meaurements were taken using a different substrate (silicon) than the microscopy based techniques. This may alter the coating thickness due to variations in the sticking probability and electrical characteristics of the substrates. Profilometry is, however, the simplest analysis to perform. SEM measurements may be subject to errors introduced through specimen tilting and lack of resolution of the the micrographs. TEM measurements may be the most

67

Table 2 - Specimen parameters

Series	Applied Bias	Sputter Clean	Thickness (A)			Failure Mode	Failure Load (MPa)
			α-Step	SEM	TEM		
II	0.0 kV	No	1650	2000	1300	Ni/Cord.	4.88
	2.0	No	3500	5000	4900	Ni/Cord.	27.44.
	4.0	No	2700	9000	4800	Mixed	38.02
III	0.0 kV	Yes			1125	No Fails	71.02
	2.0	Yes				Ni/Cord.	18.96
	3.0	Yes		8000	6700	Ni/Cord.	9.79
IV	0.0 kV	No	8500	8100		Ni/Cord.	7.65
	0.0	Yes	6600	4600		Mixed	61.16
	3.0	No	3600			Mixed	53.44
	3.0	Yes	3500			Ni/Cord.	28.20

68

Table 3 - Typical operating parameters

Base pressure (no working gas)		: 1 x 10^{-8} Torr
Argon flow (working gas)		: 50 sccm
Electron beam evaporator	bias	: 10 kV
	current	: .20 A
Sputter cleaning	bias	: 2.0 kV
	time	: 10 min.
Evaporation time		: 60 min.
Substrate bias	voltage	: 3.0 kV
	current	: 15 mA

accurate, but are also the most difficult to obtain. Generally,
the alpha-step values are used until they can be confirmed via
direct observation in the TEM. Variations in film thickness from
batch to batch can be attributed to differing evaporation rates
from the source and increased sputtering of the film at the
higher applied bias values.

E. MECHANICAL PROPERTIES

Adhesion data for the films in the as plated condition,
shown in table (2), primarily indicate trends in adhesive
behavior. The reader should be aware that the mode, or locus, of
the failure is the important criterion. Ni/cord failures,
generally observed at low strength values, indicate separation at
the metal/ceramic interface, while mixed mode failures represent
partial epoxy failures and partial interfacial separation. Based
on this consideration, two major observations can be drawn: high
applied bias is necessary to promote adhesion on a non sputter
cleaned substrate; while the use of an applied bias during
deposition onto a sputter cleaned substrate degrades the adhesion
strength. These observations, taken from series II and III
results individually, were substantiated by analysis of the
series IV samples. The data from the post thermal cycle adhesion
tests, shown in table (4), is a representation of the stability
of the metal/ceramic bond. Although the use of a 4.0 kilovolt
bias is adequate to provide adhesion to a non sputter cleaned
substrate, it is not sufficient to give thermal stability to the
bond. Films deposited, without the use of an applied bias, on

70

Table 4 — Post thermal cycle adhesion results

Series	Applied Bias	Sputter Clean	Atmosphere	Failure Mode	Failure Load (MPa)
II	0.0 kV	No	100% Argon	Ni/Cord.	0.0
	0.0	No	10 H_2 – 90 Ar	Ni/Cord.	0.0
	2.0	No	100% Argon	Ni/Cord.	8.89
	2.0	No	10 H_2 – 90 Ar	Ni/Cord.	0.69
	4.0	No	100% Argon	Ni/Cord.	8.14
	4.0	No	10 H_2 – 90 Ar	Ni/Cord.	0.0
III	0.0 kV	Yes	10 H_2 – 90 Ar	Mixed	41.80

sputter cleaned substrates are, on the other hand, able to withstand thermal cycling in a chemically reducing atmosphere. Four point bend test results for coated and uncoated cordierite, evaluating the mechanical strength of the cordierite as a function of processing, are given in table (5). Polished cordierite is shown to be stronger than the as received cordierite, but not to a large extent - indicating no major changes in the substrate as a result of polishing. Analysis of coated, polished substrates - with the films deposited under typical operating conditions, with no applied bias - shows a large difference in strength, depending on whether or not the substrate was sputter cleaned prior to deposition. Substrates which were sputter cleaned before coating retained strength equivalent to uncoated substrates, while those which were not exhibited a significant decrease in strength.

F. ELECTRON MICROSCOPY

The scanning electron micrographs (figures 18-20) give some indication of the morphology and thickness of the coatings. The nickel coating deposited without the use of an applied bias onto a non sputter cleaned substrate (figure 18) exhibits a distinctive columnar structure, with an accompanying domed surface. This is a typical example of a zone 1 morphology. When a similar coating is grown at zero applied bias on a sputter cleaned surface (figure 19) the surface topography becomes less evident and the columns less well defined, indicating a transition away from the zone 1 morphology. The addition of a

72

Table 5 - Four point bend results

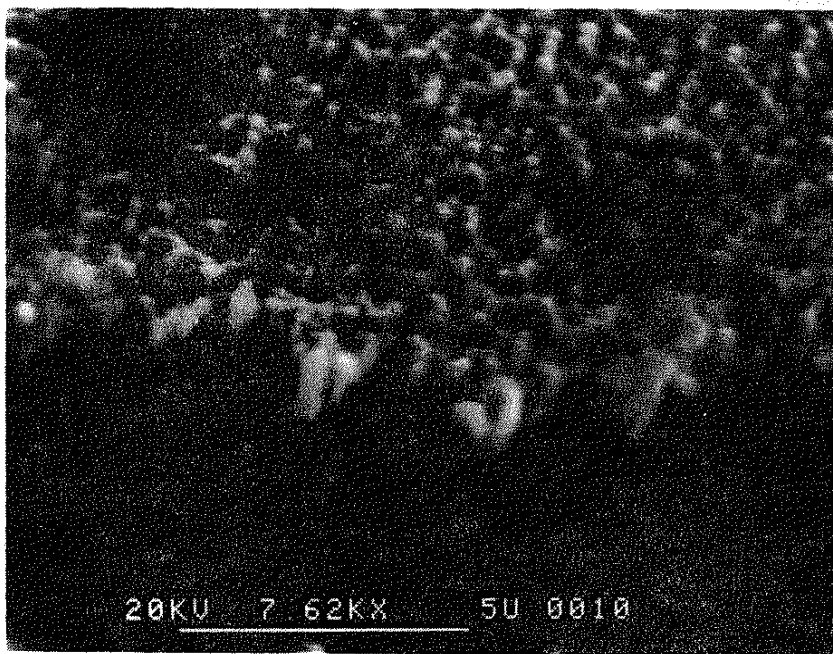| Sample description	Breaking strength (MPa)
As received cordierite	175.0 +/- 37.7
Polished cordierite	194.4 +/- 23.2
Nickel coated cordierite	
polished, sputter cleaned	181.9 +/- 18.1
polished, not sputter cleaned	122.2 +/- 3.1

Figure 18 – Scanning electron micrograph of a
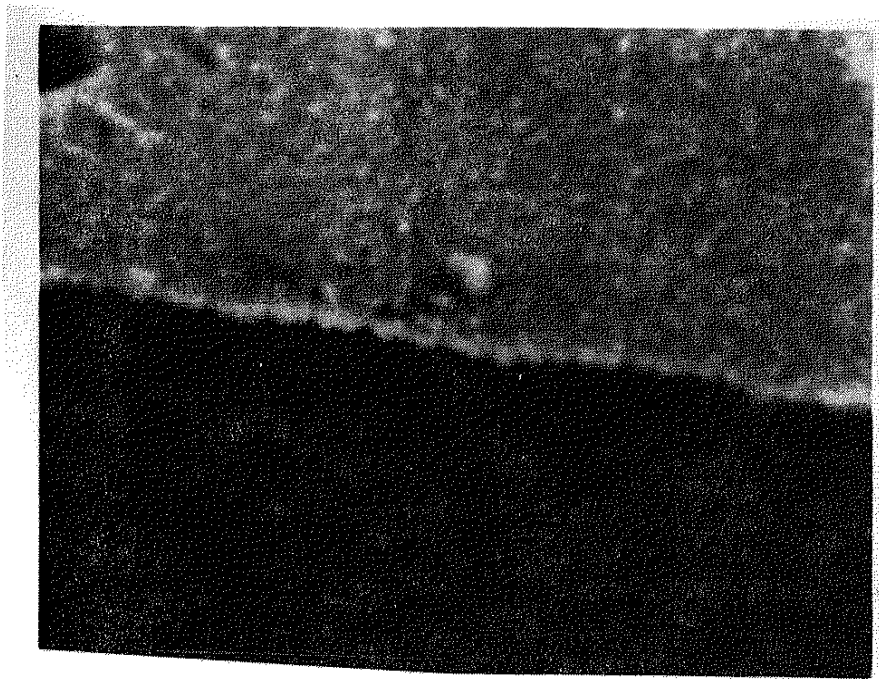nickel film on a polished
cordierite substrate (0.0 kV
bias)

Figure 19 - SEM of nickel film on polished,
sputter cleaned cordierite (0.0
kV bias)

75

Figure 20 - SEM of nickel film on polished,
        sputter cleaned cordierite (3.0
        kV bias)

3.0 kV bias to the situation (figure 20) does not seem to alter the morphology significantly. Since these three coatings exhibited widely different adhesive behavior, examination on a much finer scale is required to relate the structure to the properties.

Figures (21-29) comprise a transmission electron microscope analysis of cross sections of nickel/cordierite couples. Figures (21-27) are from films grown on polished cordierite substrates which were not sputter cleaned prior to deposition, while the substrate for figures (28,29) was sputter cleaned. Figure (21) shows a nickel film deposited without an applied bias, exhibiting a fine grained initial nucleation layer and a columnar morphology. Some evidence of the domed surface (tops of columns) is also present. Figures (22-25) are a series of micrographs taken from a film deposited with a 2.0 kV applied bias. Figure (22) shows the columnar morphology of the film, the microstructure of the cordierite, and some indication of the fine grained nucleation layer similar to the 0.0 kV case. Note that there is some separation visible between columns, as well as a "modification" in the near interfacial cordierite morphology. Figures (23,24) are a bright field - dark field pair of the 2.0 kV film showing the growth morphology of the film and the morphology of the substrate. The polycrystalline nature of the columns is demonstrated (especially in the dark field micrograph), as is the internal structure of the individual grains. Note that although the morphology is still primarily columnar, the columns are not as well defined as in the 0.0 kV
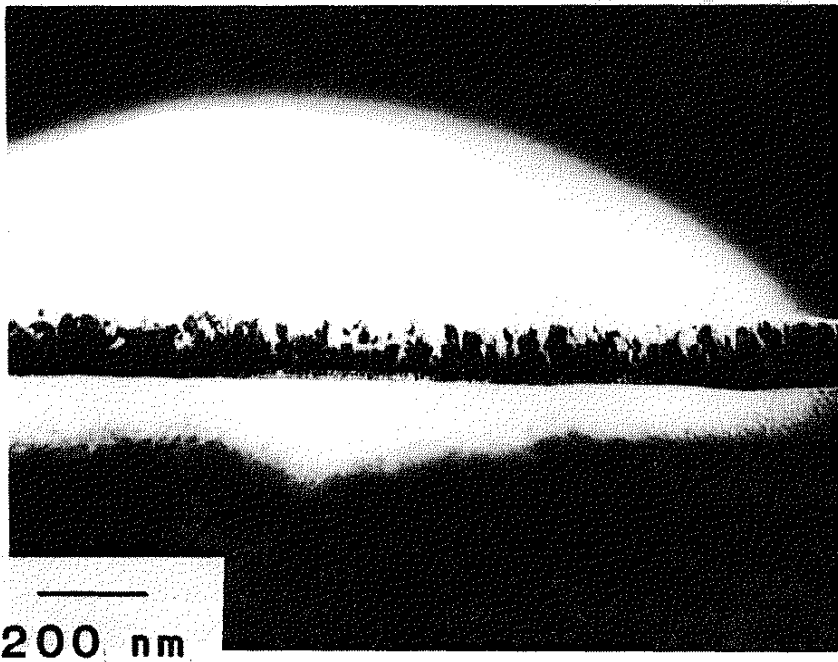
200 nm

Figure 21 - TEM micrograph of 0.0 kV nickel
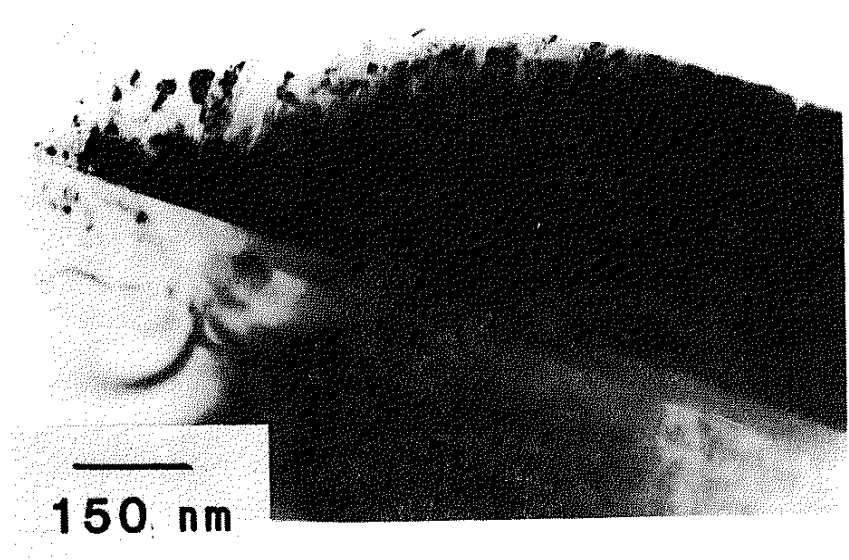film on polished, non sputter
cleaned cordierite

150 nm

Figure 22 - TEM of 2.0 kV nickel on polished,
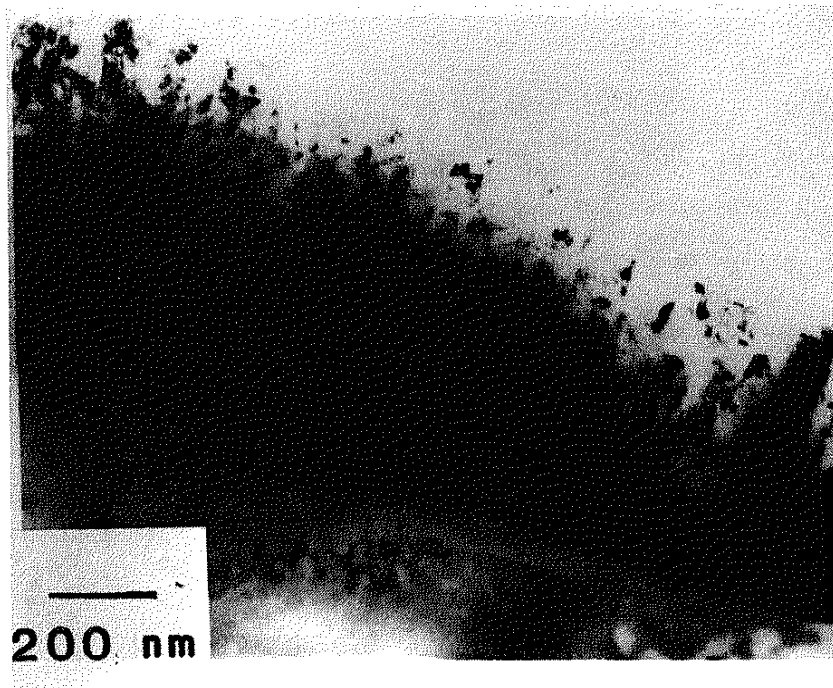non sputter cleaned cordierite

200 nm

Figure 23 - TEM of 2.0 kV nickel on polished,
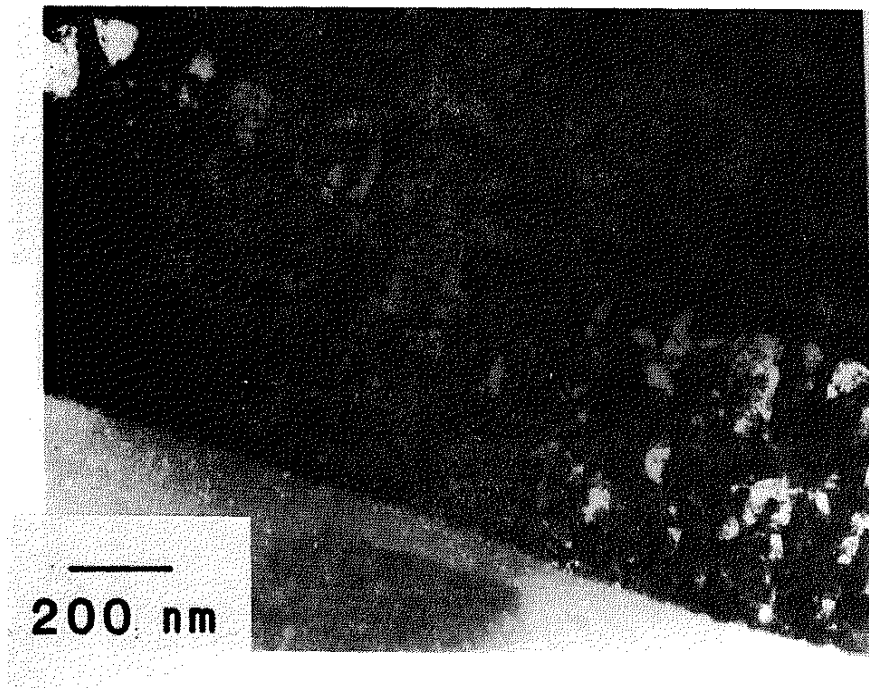non sputter cleaned cordierite
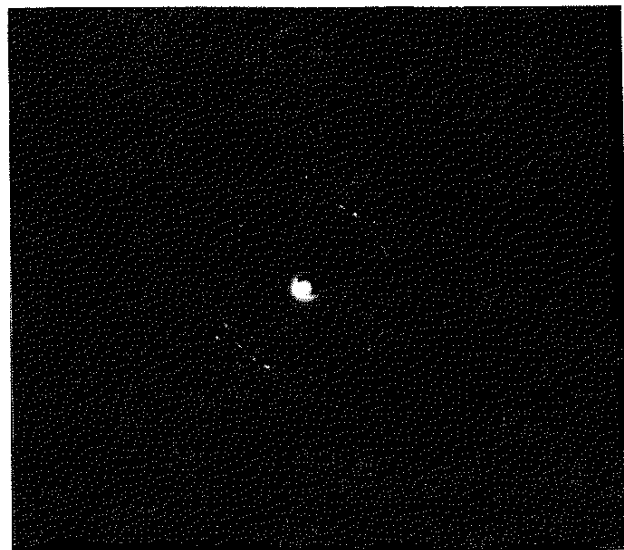(bright field)

Figure 24 - Dark field corresponding to figure 23

Figure 25 - Selected area diffraction pattern
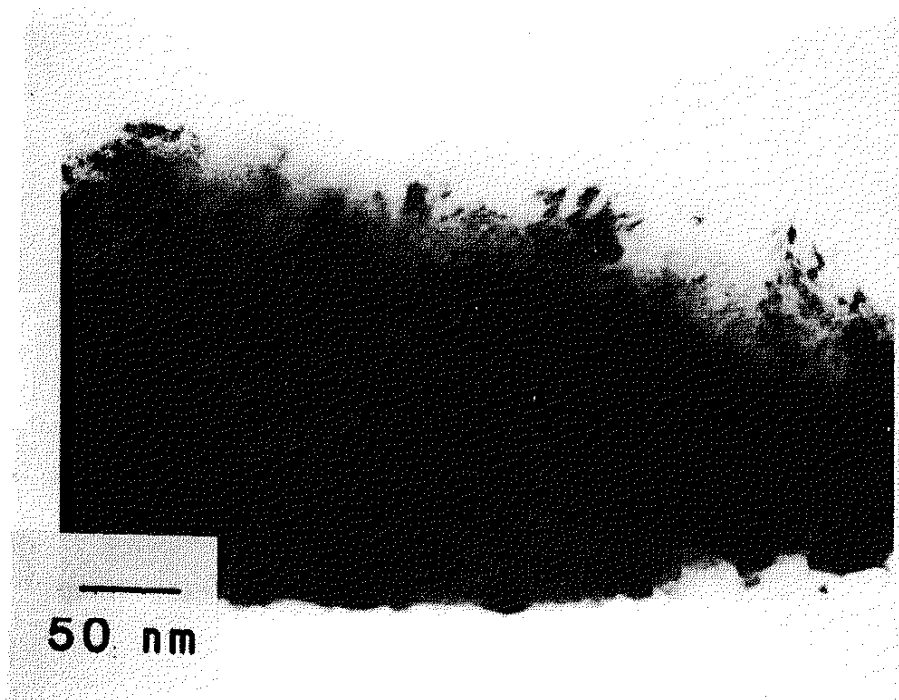from 2.0 kV nickel film on
polished, non sputter cleaned
cordierite

50 nm

Figure 26 — TEM of 4.0 kV film after being detatched from the substrate (no sputter cleaning, polished)
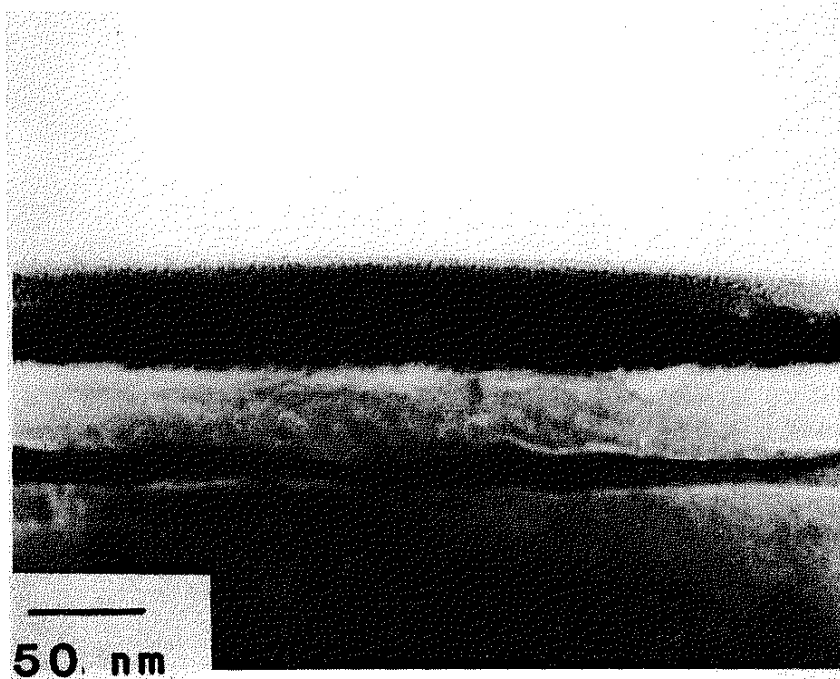
Figure 27 - Polished cordierite substrate
after 4.0 kV deposition (no
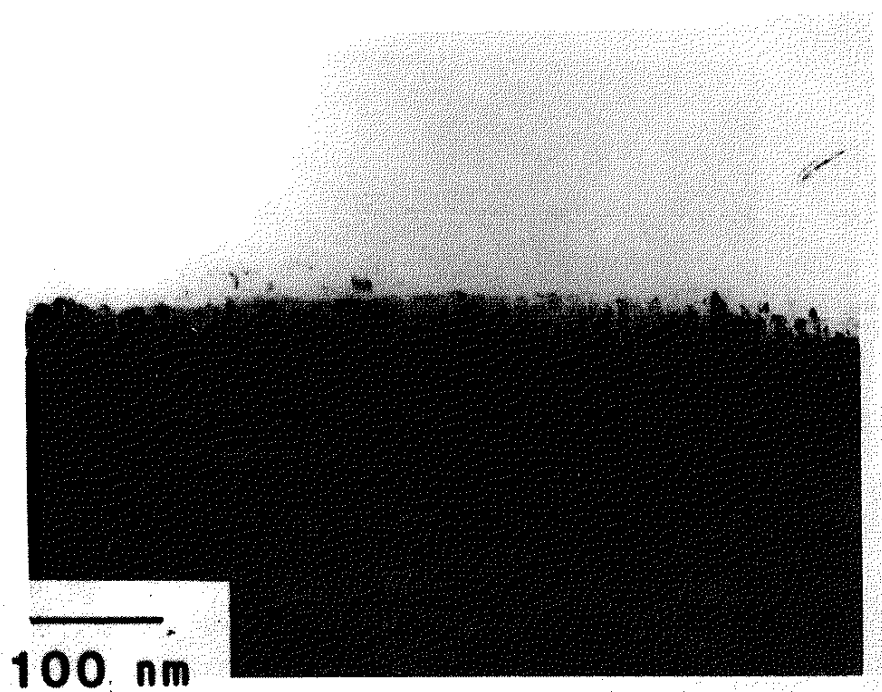sputter cleaning, film removed)

Figure 28 - TEM of nickel film deposited at
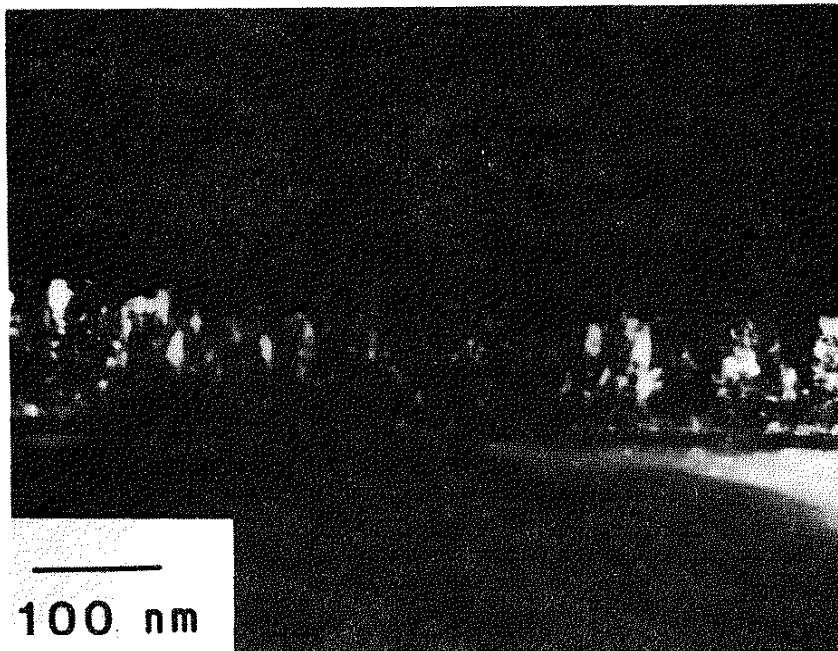0.0 kV on a polished, sputter
cleaned substrate (bright field)

Figure 29 - Dark field corresponding to
figure 28.

case. Figure (25) is a selected area diffraction pattern from the film, indicating its random polycrystalline nature. Table (6) lists the crystallographic planes of the nickel corresponding to the first six reflections in the pattern. Figure (26) shows a portion of a film, deposited at 4.0 kilovolts, which had been detatched from its substrate during specimen preparation. Note the transition to an equiaxed grain structure, along with an accompanying increase in film density. Figure (27) is the substrate corresponding to figure (26). The presence of the various layers is thought to be a consequence of the energetic deposition process. Investigations are underway in order to attempt to characterize the individual regions both structurally and chemically. The small circular features present are determined to be nuclei of amorphous regions in the cordierite, resulting from damage due to analysis using a highly focussed beam of electrons (small spot size) in the TEM. Figures (28,29), films deposited at 0.0 kV on a sputter cleaned substrate, show a similar growth morphology to the non sputter cleaned case, with the exception of the modified ceramic zone. The film morphology is clearly columnar, with significant amounts of separation present between columns. There is an initial nucleation layer present, as well as an "altered" layer in the cordierite. The layer is identified as being ceramic by virtue of its contrast in dark field. It also differs in appearence from the altered layers described previously, and may be the explanation behind the extremely high adhesion strength of this sample. Note that the bright spots above the film in dark field are from the epoxy

87

Table 6 - Nickel diffraction pattern analysis

Ring Number	Crystallographic plane
1	111
2	200
3	220
4	311
5	222
6	400

used in specimen preparation which remained in place, indicating the film is intact for its full thickness.

Microchemical results obtained via energy dispersive x-ray analysis in the scanning transmission electron microscope are presented in figures (30-37). Figures (30-33) are from a film grown on a sputter cleaned substrate without an applied bias, while figures (34-37) are from a film deposited with a 2.0 kilovolt bias on a substrate which was not sputter cleaned. The first two figures show the representative compositions on either side of the nickel/cordierite interface, indicating there is some amount of chemical mixing present. Figures (32,33) are plots of the composition in two of the altered substrate regions seen in figure (28). Figure (32) is from the light band nearest the interface, with figure (33) being from the dark band adjacent to it in the substrate. Although the two regions exhibit markedly different contrast, their chemical compositions are almost identical. The only variation is that the band nearer to the film has a slightly higher nickel content, as expected from diffusion. There is, however, no discontinuous transition in composition from one layer to the other. This indicates that the differences may be structural as opposed to chemical. The last series of plots (figures 34-37) demonstrate the change in composition across the interface. Note the unusual composition of the cordierite in these scans; with the silicon being enhanced and the the aluminum depleted. This behavior was observed at all points along the interface of this specimen.

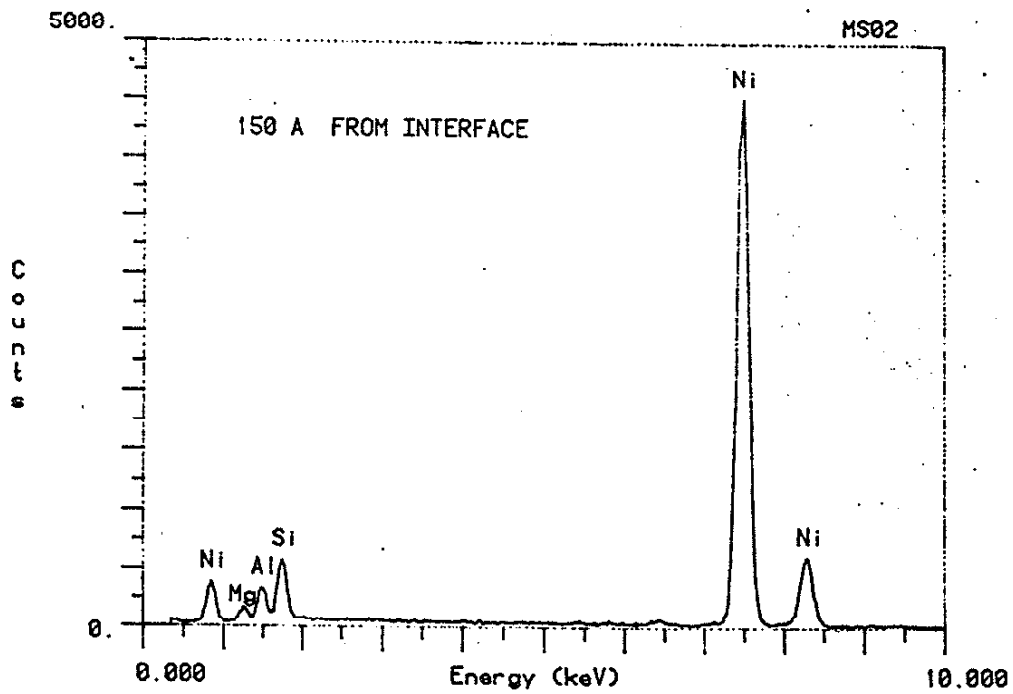The TEM analysis, though difficult to conduct due to

89

Figure 30 — EDS scan of nickel film near
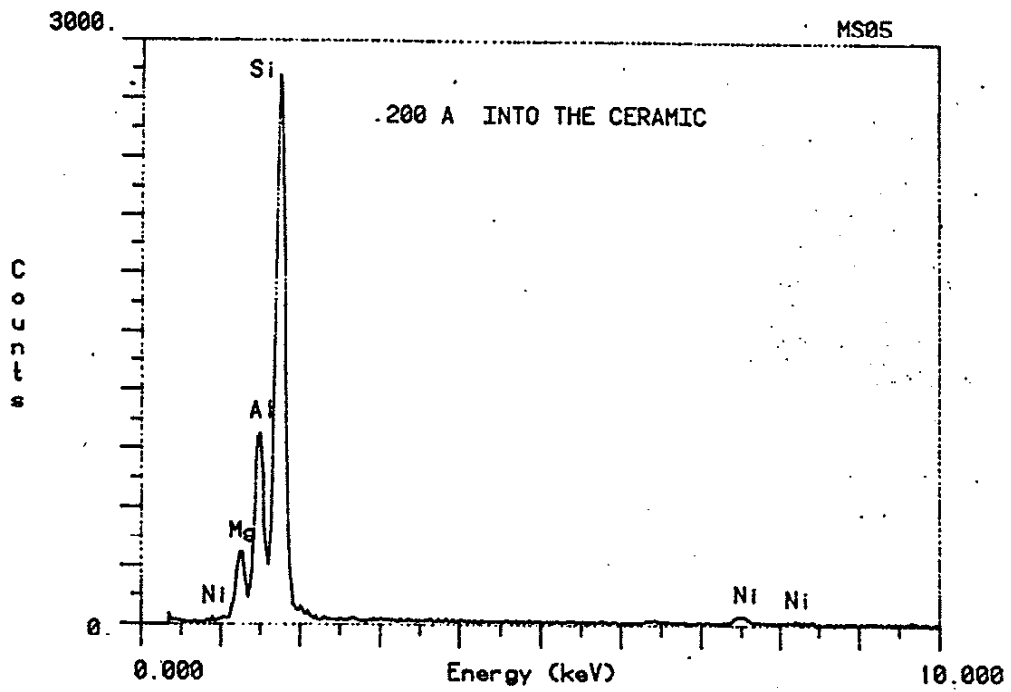interface (0.0 kV, sputter
cleaned)

Figure 31 — EDS scan of substrate near
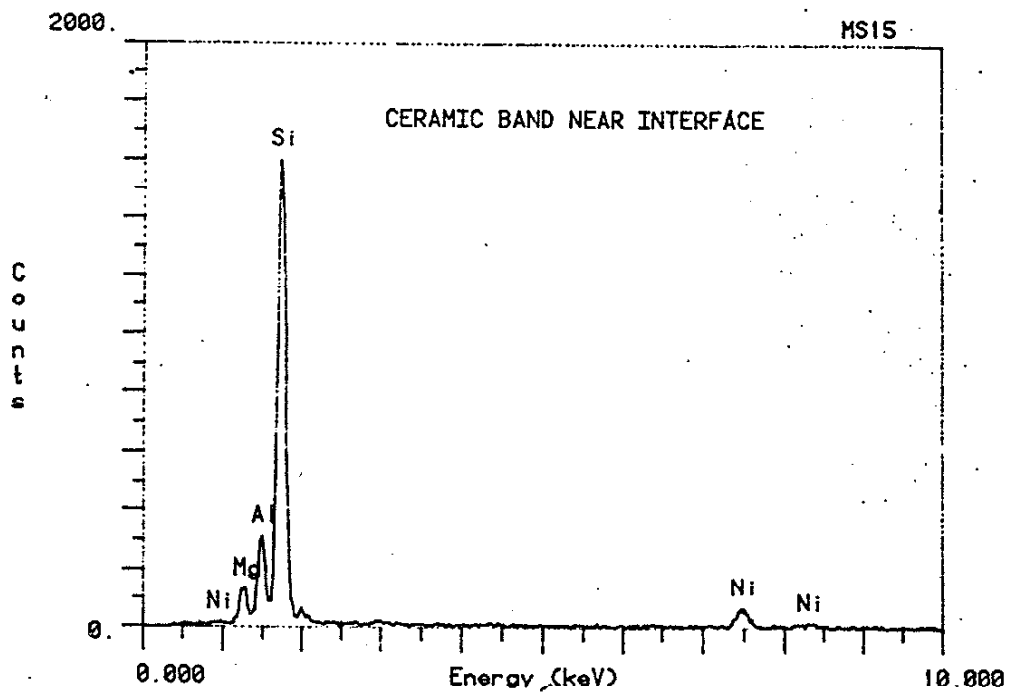interface (0.0 kV, sputter
cleaned)

Figure 32 - EDS scan of altered layer next to
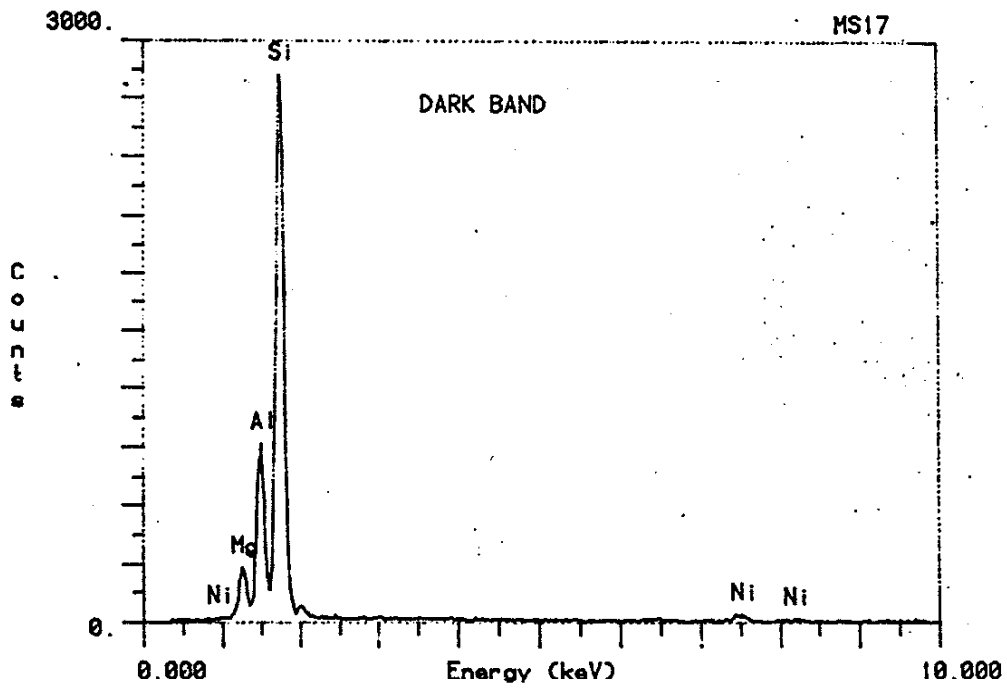interface (0.0 kV, sputter cleaned)

Figure 33 - EDS scan of second altered layer
in the substrate (0.0 kV, sputter
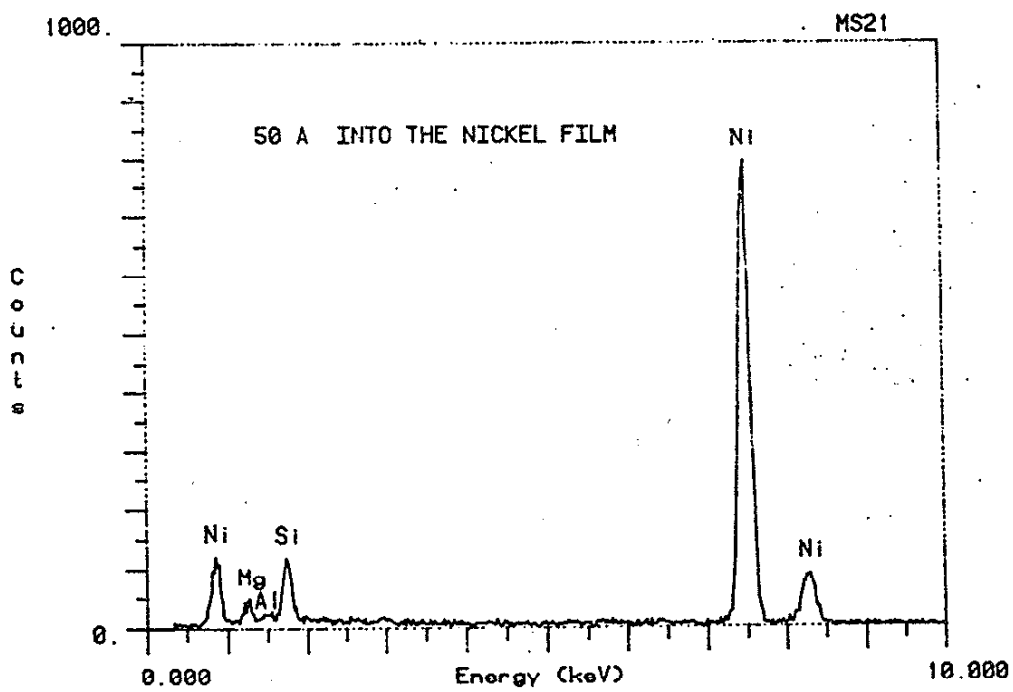cleaned)

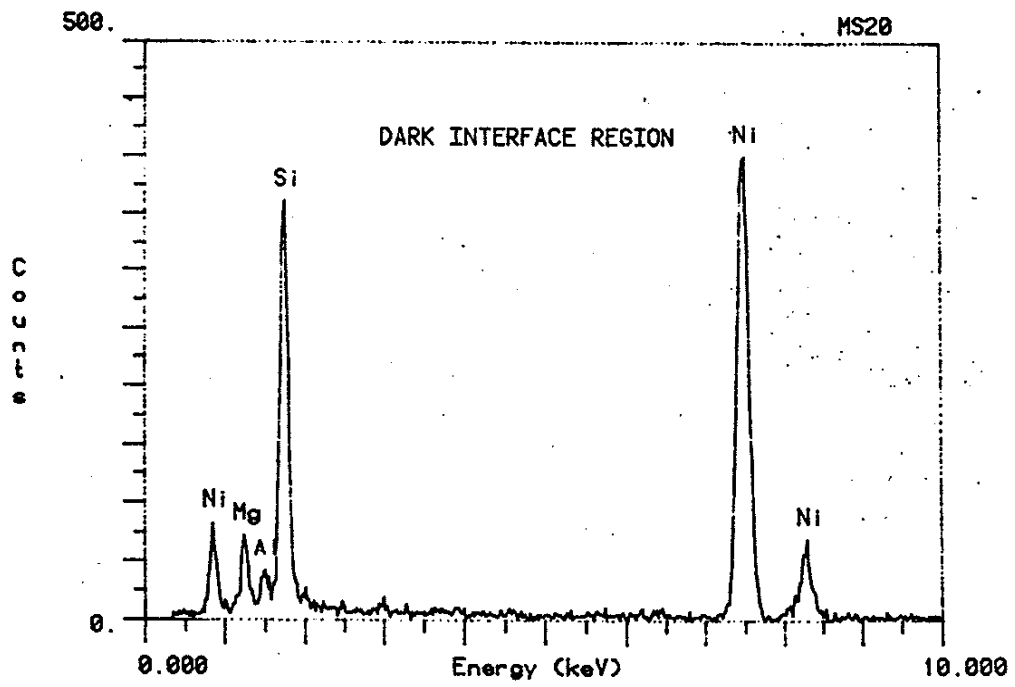Figure 34 - EDS scan, 2.0 kV film, no sputter
cleaning

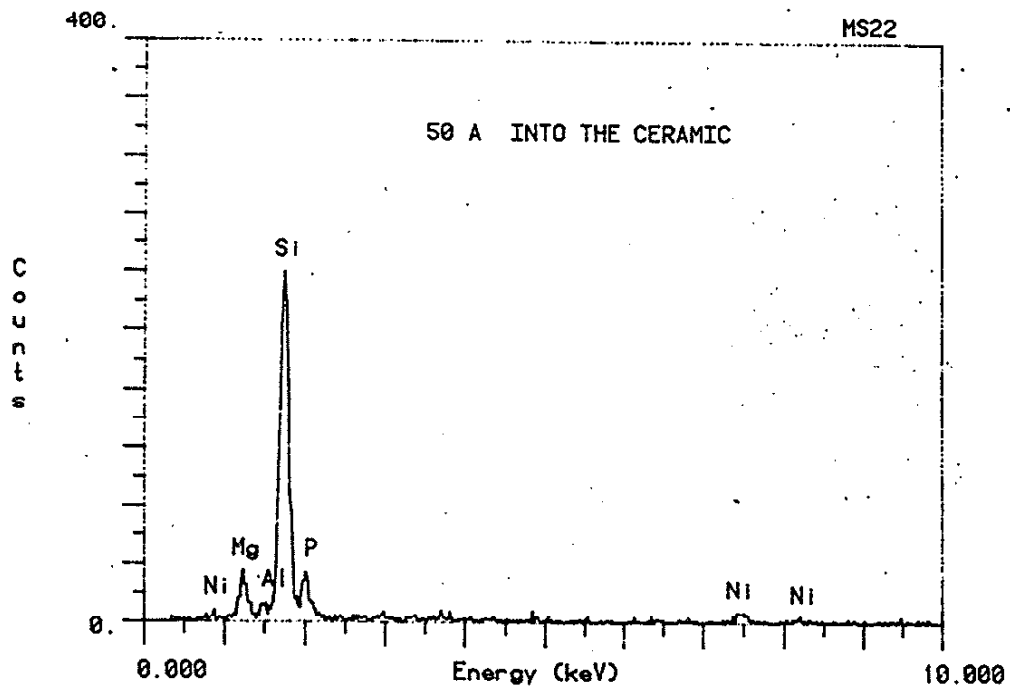Figure 35 – EDS scan, 2.0 kV film, no sputter
cleaning

95

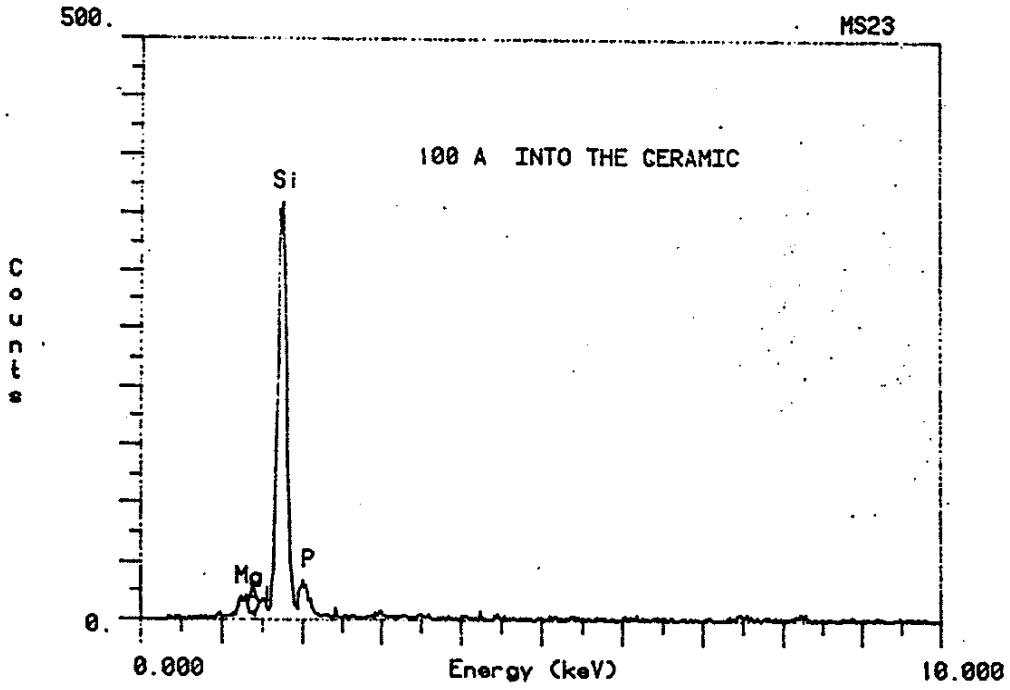Figure 36 - EDS scan, 2.0 kV film, no sputter
cleaning

Figure 37 - EDS scan, 2.0 kv film, no sputter
cleaning

specimen preparation limitations, has nonetheless provided direct insights into the structure and chemistry of the system. Film morphology is shown to progress from zone 1 (columnar) to zone 3 (equiaxed) with applied bias; the presence of various layers on either side of the interface is detected; and variations in local microchemistry have been documented. A large number of results have been presented here, but they do not reveal the final answers. Ongoing research is being concentrated most heavily in the area of transmission electron microscopy.

G. SURFACE CHEMISTRY

Although microchemical analysis in the TEM has the inherent advantage of being able to analyze very small specific areas of interest, surface chemical analysis in the Auger microprobe and SIMS, when used in conjunction with depth profiling, can provide useful information without the need for elaborate specimen preparation. Figure (38) is an Auger survey scan of a representative nickel film, taken after surface contaminants from handling and cutting were sputtered away, showing the cleanliness (purity) of the film. No transition metal elements were detected — a direct result of coating all exposed parts of the chamber with nickel prior to actual film growth. The need for the coating of the chamber is demonstrated in figure (39), an Auger scan of a polished cordierite substrate subjected to the standard sputter cleaning operation. The presence of copper, as opposed to nickel, is due to the plating system being coated with copper for another investigator at the time the experiment was
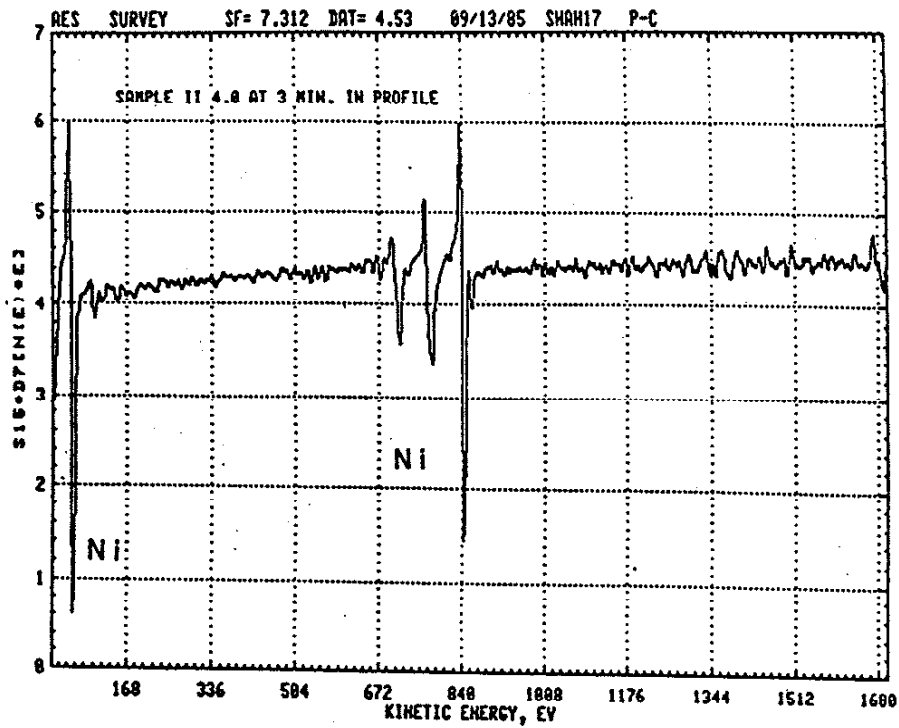
Figure 38 — Auger survey scan of a representative nickel film
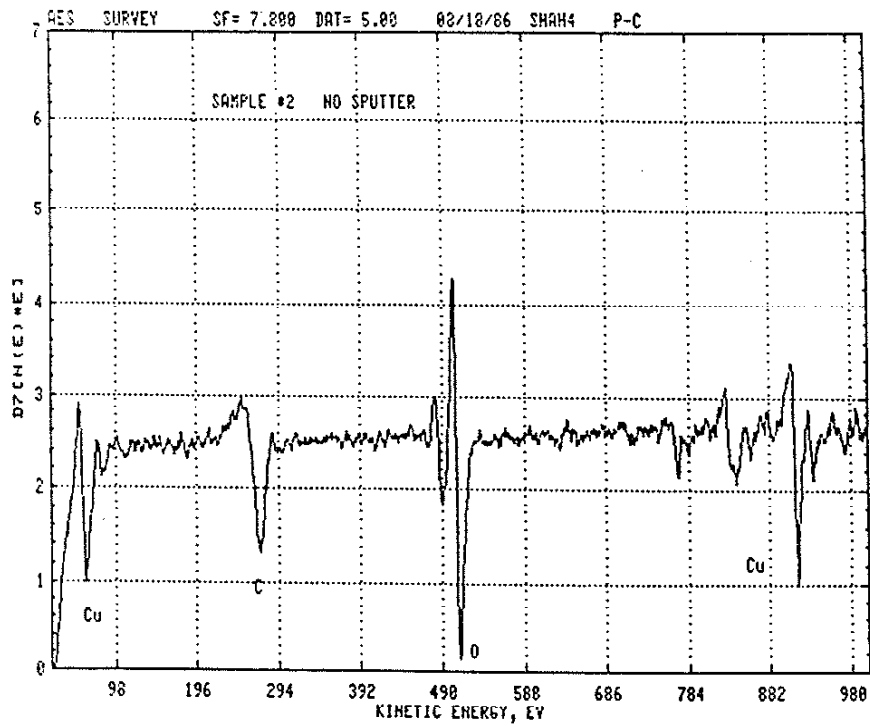
Figure 39 - Auger survey scan of polished
cordierite substrate after
sputter cleaning

conducted. This indicates that, for the case of sputter cleaned

substrates, deposition is occuring on an alloyed (doped) surface.

The composition vs depth profile shown in figure (40) is designed

to yield the width of the chemically mixed interfacial region.

Profiles were taken for samples deposited under various

processing conditions, but no variations in interface width were

detected, within experimental accuracy. The SIMS "reverse

profile" shown in figure (41) also demonstrates the presence of a

chemically mixed interface. Since the film was removed from the

substrate prior to profiling, all elements detected must have

been present on the film side of the interfacial separation and

not artificially induced. Depth profiles were used in addition

to survey scans since the decrease in concentration of the

substrate elements with depth was further proof of their

authenticity.

AES   PROFILE   09/13/85 SHAH16   P-C

SAMPLE II 4.0

Figure 40 - Auger depth profile of nickel
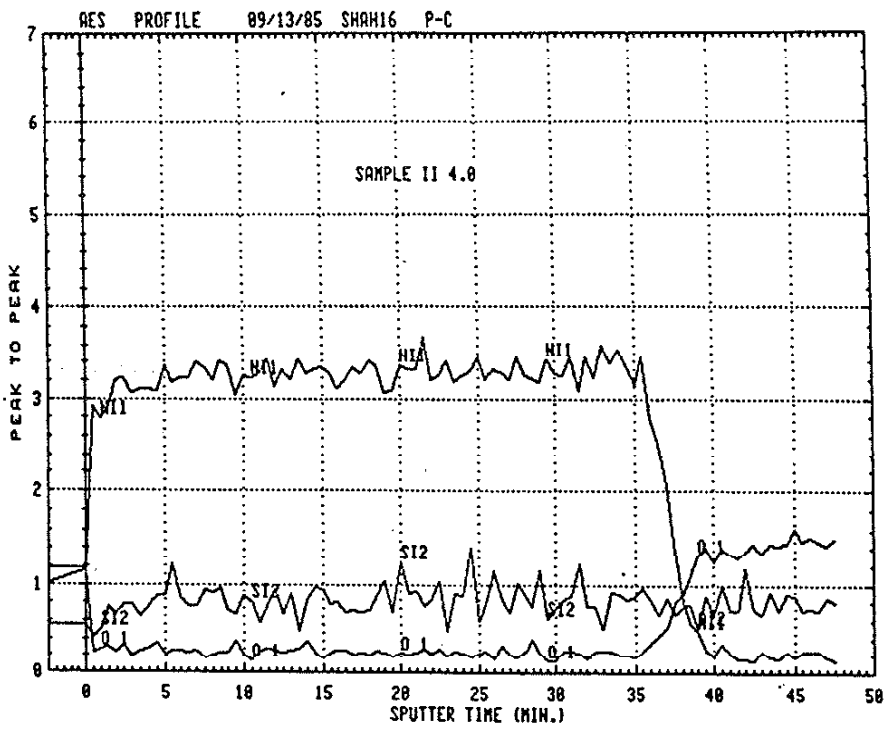   film (4.0 kV) on a non sputter
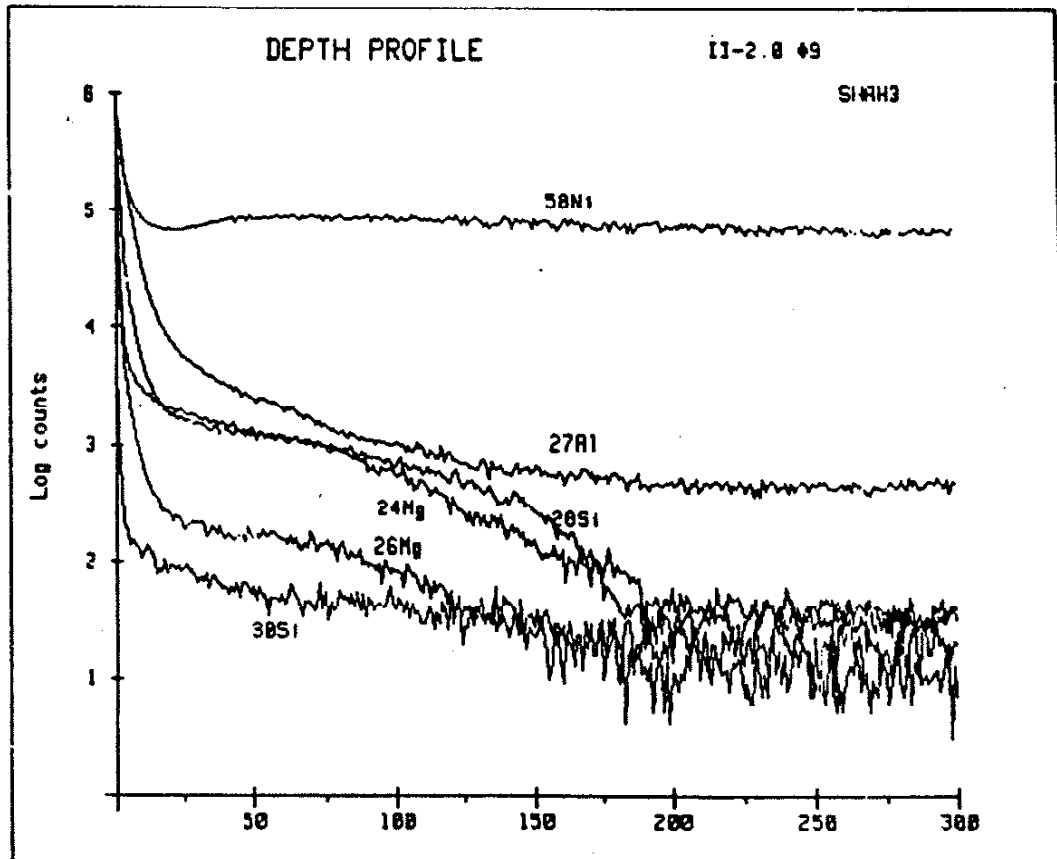   cleaned substrate

Figure 41 – SIMS reverse profile of a 2.0 kV
nickel film removed from the
substrate

VI. DISCUSSION

A. SUBSTRATE PREPARATION

Substrate polishing reduced the background surface roughness by approximately an order of magnitude, from 250 nm to 25 nm, while subsequent sputter cleaning smoothed out the tops of some of the finer remaining hillocks. The mechanical polishing procedure employed in this study served a variety of purposes, most important of which is the establishment of a well characterized, reproducible starting point for deposition. This concept was emphasized in the review of substrate preparation presented by Mattox [55]. Reducing the background roughness was also necessary since the as received roughness was on the order of the coating thickness, making it difficult to grow a uniform, continuous film. Polishing also aided the analysis of the film/substrate couple. SEM fracture sections could be obtained, showing a smooth film/substrate interface at the magnifications utilized. Auger depth profiling required a smooth interface to improve the depth resolution due the beam averaging over a given area of the surface. It was hoped that polishing would provide a smooth enough surface to obtain coating thickness measurements via alpha-step profilometry, but this was not the case.

Sputter cleaning of the substrate in situ prior to deposition did not do much to change the overall topography of the surface, but did alter its chemistry. The slight decrease in surface topography detected (rounding or removal of the tops of the finer hillocks) is contrary to the effect described by Mattox

[33], who predicted an increase in roughness. An opposite view could be taken by considering the increased probability that a hillock may have over a valley for being struck by an incoming particle. Sputter cleaning is expected to remove surface contaminants [55] and provide an atomically clean surface [35], but contamination due to backsputtering can be a problem [5]. The effect of backsputtering was confirmed in this investigation by examining the surface of a sputter cleaned substrate via Auger electron spectroscopy. The surface was doped with the material used to coat the chamber; the same material as the evaporant is used so as to avoid contamination of the film or interface. This "alloying" of the surface may be beneficial, as indicated by the adhesion results of this study. Stroud [7] agrees by introducing the idea of implanting a surface to give a reactive layer which may be metastable and/or contain metal ions for bonding. Modification of the surface and interface chemistry to enhance adhesion was described by Mattox as well [5]. Microstructural effects of sputter cleaning will be discussed in a later section in conjunction with the effects of energetic particle bombardment.

B. PROPERTIES

Although three methods for thickness analysis were employed, significant variations among the techniques were observed. Most of the observed variation can be attributed to experimental difficulty. As mentioned in the previous section, polishing of the cordierite substrates did not provide a smooth enough surface

105

for profilometry. The problem of noise due to surface roughness making it unable to obtain accurate traces over a step in the coating was described by Piegari and Masetti [56], who suggested averaging of the traces, as done in newer computer aided profilometers, as a possible solution. The method adopted in this investigation was to insert overlapping pieces of highly polished silicon into the chamber and take measurements from these, as opposed to the cordierite. Because the dependence of net deposition rate (evaporation minus sputtering) as a function of substrate type is not fully known, it is believed that using silicon could be a major reason for the discrepancies in the readings, especially at the higher bias voltages where sputtering is more prevalent. This applied bias effect was observed in this study. Piegari and Masetti [56] were also concerned with the ability to obtain a sharp step in the coating, however this was satisfied by ensuring the two pieces of silicon were in close contact. SEM thickness measurements were not often used because of the geometrical distortions arising from tilting the sample to obtain a good image. TEM is the method of choice, since a direct observation of the film is provided. The utility of this method is limited by specimen preparation requirements, especially for thicker films (> 1 micron) where it is difficult to obtain thin area at the interface while maintaining the entire coating thickness intact.

Coating adhesion was enhanced by increasing the applied bias during deposition if the substrate was not sputter cleaned, but was degraded if a bias is applied during deposition on a sputter

cleaned substrate. Optimal adhesion was obtained by growing the
film on a sputter cleaned substrated without the use of an
applied bias. This was also the only condition which resulted in
a film that was thermally stable in a chemically reducing
atmosphere. Increased film adhesion is one of the inherent
advantages of the ion plating process, and is generally accepted
to be a result of energetic particle bombardment from the glow
discharge producing a graded interface and more active nucleation
sites. Based on this premise, the results for the non sputter
cleaned substrates were as expected. The increased adhesion due
to the use of a glow discharge has been confirmed by Stoddart et.
al. [15], Perry and Pulker [17], and Swaroop and Adler [24]. In
order to increase adhesion for all applied bias values, sputter
cleaning was introduced to the process. Sputter cleaning is
thought to improve adhesion by the mechanisms described in the
previous section and the background review on ion plating, and
was observed for the copper on cordierite system by Scott [57] in
this laboratory. The results obtained for nickel deposited on
sputter cleaned cordierite were, however, anomalous. Sputter
cleaning did provide good adhesion to the 0.0 kV films, as
expected. When a bias was used during deposition, the adhesion
diminished. This decrease in adhesion with increasing bias has
not been reported elsewhere in the literature, and has not been
fully explained in this study. A possible explanation is the
alteration in the stress state or nucleation behavior at the
interface. Residual stresses between the film and substrate can
cause premature failure of the bond [12]. Sputter cleaning seems

to be a major factor in adhesion, but is very seldom used as an experimental variable. Microstructural and microchemical data, discussed later, may shed some light on the analysis.

The Sebastian adhesion test did provide useful information concerning bond strengths, but fell short in its ability to give accurate quantitative data. As was reported by Mirtich [21] and Salem and Sequeda [22] for their analyses, the strength of the Sebastian epoxy was a limiting factor in this examination. Scatter in the data, even at low strength values and complete interfacial failure, was sufficient to cast doubt over the reliability of the failure load data. The locus of the failure was determined to be the important criterion in this study, as suggested by Mittal [11] in his review on adhesion.

The four point bend test was primarily employed to evaluate the mechanical strength of the cordierite following ion implantation (appendix C), but was also used to examine the effects of polishing and sputter cleaning. Polishing did improve the breaking strength, as expected due to the reduction in the number and size of surface defects, which can act as failure initiation sites. Coated substrates which were sputter cleaned before deposition showed much greater strength than those which were not, lending evidence to the idea of a change in the stress state at the interface. The limited results of the four point bend tests to date are in accord with the adhesion data.

C. STRUCTURE

Scanning electron microscopy of the nickel films indicated a

transition from a well defined columnar structure with domed tops (zone 1) to a more dense, less columnar structure with little surface topography (zone 2) as the energy of the depostion is increased. The 0.0 kV film on a non sputter cleaned substrate exhibits the classic zone 1 structure [47], as expected since the parameters used are identical to thermal evaporation, with the exception of the gas scattering present. The progression toward the higher temperature zone T morphology [48] when sputter cleaning is performed is a manifestation of the energertic particle bombardment from the glow discharge. Sputter cleaning has been said by Mattox to alter the nucleation and subsequent growth behavior of a film [5]. The morphologies are still similar, since no bombardment occurred during growth in either case. Addition of a 3.0 kV bias during deposition did not alter the morphology significantly, but did result in a more distinct zone 2 structure than the 0.0 kV sputter cleaned film. The ability to achieve these "high temperature" morphologies at room temperature is one of the attributes of ion plating. The results obtained in this study were in agreement with the zone diagram predictions of Movchan and Demchishin [47] and Thornton [48,49]. They also agree with experimental investigations by Pulker et. al. [53], Enomoto and Matsubara [51], and Minni and Sundquist [52]. Minni and Sundquist reported a columnar structure for evaporated films, with an increasing number of interruptions in the columnar growth as the cathode current was increased. This was said to be due to an increase in the number of active nucleation sites as a result of ion bombardment. For the small

film thicknesses (< 1 μm) encountered in this investigation, interpretation of the SEM micrographs becomes somewhat subjective. Confirmation of the observed morphologies via TEM is a requirement.

Transmission electron microscopy, despite its difficult sample preparation, was a primary focus of this investigation by virtue of its unique abilities. While most investigators in the ion plating field examine their films via SEM, no examples of TEM investigtions were found. Cross section TEM analysis did confirm the film morphologies recorded in the SEM, but also revealed the presence of various layers in the film and substrate. Although SEM revealed a very regular columnar morphology for a 0.0 kV film deposited without sputter cleaning, TEM indicated that the columns actually grow out of a fine grained, equiaxed nucleation layer. The presence of a nucleation layer, though on a much larger scale, was also reported by Enomoto and Matsubara [51] for copper on tungsten. In both studies, the nucleation layer was most evident under conditions of low (or zero) applied bias. No conclusive explanation for this phenomenon has yet been formulated. In addition to the transition from a columnar to an equiaxed grain structure as the bias is increased, a corresponding increase in film density is observed. One of the most important features detected by the TEM is the "modification" of the ceramic surface during processing. Layers of varying contrast are seen if the substrate has been exposed to a glow discharge; either during sputter cleaning or during film growth. It is thought that these layers are the controlling factor in

film adhesion. The concept of interface layers in metal/ceramic bonds is not new - Petzow et. al. [8] reported spinel formation in copper/alumina systems - but they mostly result from high temperature processing. Direct structural characterization is the ideal analysis to perform on these layers, but progress has been slowed by the structural instability of the cordierite substrate. When subjected to a highly focussed electron beam, as is the case with conventional microdiffraction and CBED, the cordierite undergoes a crystalline to amorphous transformation. This may necessitate real time diffraction analysis, perhaps with the aid of a video camera system. Chemical analysis of some of the layers has begun, and will be discussed in the following section.

D. CHEMISTRY

Microchemical analysis was used primarily to obtain information on the elemental composition of the interface region, but was also used to qualify the chemistry of the film and substrate. The films were found to have no significant contamination, via Auger electron spectroscopy. Auger depth profiling techniques did provide interfacial width values, but their validity is questioned by virtue of there being no variation in width as a function of processing conditions. This same method of interface analysis was used by Minni and Sundquist [52], who stated that the interface became broader at higher cathode current densities. No quantitative evaluation of their depth profiles is given, however. The "effective" depth

111

resolution of Auger profiling for interface studies is something which must be considered in light of problems with surface roughness and film thickness variations. Interface widths in the current study may be less than the practical experimental resolution. Sputtering done by the instrument in order to profile into the sample can cause recoil mixing and preferential sputtering, which can broaden the apparent interface. Surface topography can decrease the depth resolution of the profile, since one portion of the beam may see the substrate while another sees nickel deposited in a crevice; resulting in a distortion of the average compositions. Confirmation of the mixed chemistry across an adhesion failure surface was done by SIMS "reverse profiling", which was not subject to instrumentally induced mixing since the substrate is removed prior to the analysis. This mixed chemistry, or graded interface, is the expected result based on the energetic processes associated with ion plating. The most conclusive evidence of interfacial chemistry was obtained via energy dispersive spectroscopy (EDS) in the STEM. This allowed information to be derived from a highly localized (approximately 50 A) area by placing the probe on the area of interest, while maintaining an image of the field of view. Mixed chemistry is indisputably identified for a 0.0 kV film on a sputter cleaned substrate. Chemistry of the two neighboring interface layers is shown not to vary, pointing to the possibility of structural differences. This also discounts the presence of an interfacial compound, as found by Petzow et. al. [8]. For a 2.0 kV film deposited without sputter cleaning, the

112

ceramic chemistry is shown to vary from the normal stoichiometry. An aluminum depleted, silicon rich layer is found. The cause for this compositional fluctuation is not known, but enhanced diffusion is a possibility. Although the EDS evaluation is a recent addition to the analytical program, initial results are encouraging and a major effort shall be put forth in this area.

VII. CONCLUSIONS

Polishing of the cordierite substrates prior to film growth provided a reproducible, well characterized surface, with a 25 nm background roughness (an order of magnitude improvement over the as received surface), allowing continuous films to be deposited and analyzed. Adhesion of the film to the substrate is enhanced by sputter cleaning if no applied bias is used during deposition. The use of an applied bias improves adhesion of films grown on substrates which were not sputter cleaned, but diminishes it if the substrates were sputter cleaned prior to deposition. Sputter cleaning results in a chemically doped surface region as a consequence of backsputtering from the chamber walls and fixtures. Both sputter cleaning and the use of an applied bias during deposition can cause modifications in the structure and/or chemistry of the cordierite substrates at the metal/ceramic interface. Some of the adjacent modified layers in the same specimen are shown not to differ chemically, although their contrast is different in the TEM; indicating possible structural variations. The cordierite glass-ceramic undergoes a crystalline to amorphous transformation induced by a highly focussed electron beam, limiting the ability to perform small area microstructrual analysis. Overall film morphology changes from a distinctly columnar, domed structure (zone 1) when no applied bias is used or sputter cleaning performed, to a dense, equiaxed structure (zone 3) for 4.0 kV deposition. Actual film morphology can be more complex than predicted from the zone diagrams; with fine

114

grained, equiaxed initial nucleation layers, from which the columns then originate, present in the 0.0 kV films. Mixed interfacial chemistry, characteristic of ion plating, was confirmed via Auger microprobe, SIMS, and STEM/EDS techniques. Transmission electron microscopy, despite its experimental difficulties, is determined to be the method of choice for thin film and interfacial analysis, by virtue of its ability to provide direct microstructural and microchemical information from a localized area. If the proper ion plating parameters are utilized, highly adherent nickel films may be deposited on cordierite glass-ceramic substrates.

VIII. REFERENCES

1. W.D. Grobman, J. Vac. Sci. Technol., A3(3), 725, (1985)

2. A.J. Blodgett, Jr., J. Vac. Sci. Technol., A3(3), 777, (1985)

3. A.J. Blodgett, Jr. and D.A. Barbour, IBM J. Res. Dev., 26, 30, (1982)

4. "Ceramics Packaging and Interconnections in Electronic Systems: A User's Perspective", Open Forum, The American Ceramic society, Inc., 86th Annual Meeting and Exposition, Chicago, IL, (1986)

5. D.M. Mattox, Thin Solid Films, 53, 81, (1978)

6. D.M. Mattox, Thin Solid Films, 19, 173, (1973)

7. P.T. Stroud, Thin Solid Films, 9, 273, (1972)

8. G. Petzow, T. Suga, G. Elssner and M. Turwitt, Nature and Structure of Metal-Ceramic Interfaces, in Sintered Metal-Ceramic Composites, ed. by G.S. Upadhyaya, Elsevier Science Publishers, B.V., Amsterdam, (1984), p. 3

9. I.P Arsentyeva and M.M. Ristic, The Investigation of the Bond in NiAl$_2$O$_3$ System, Ibid, p. 181

10. W.K. Wlosinski, Al$_2$O$_3$-Cr and Al$_2$O$_3$-Cu Composite Technology and Properties, Ibid, p. 483

11. K.L. Mittal in Adhesion Measurement of Thin Films, Thick Films and Bulk Coatings, ASTM STP 640, ed. by K.L. Mittal, (American Society for Testing and Materials, 1978), p. 5

12. D.M. Mattox, Ibid, p. 54

13. S.J. Jeng, C.M. Wayman, J.J. Coleman and G. Costrini, Materials Letters, 3, 3, (1985)

14. D.M. Mattox, J. Vac. Sci. Technol., 10(1), 47, (1973)

15. C.T.H. Stoddart, D.R. Clarke and C.J. Robbie, J. Adhesion, 2, 270, (1970)

16. A. Kikuchi, S. Baba and A. Kinbara, Thin Solid Films, 124, 343, (1985)

17. A.J. Perry and H.K. Pulker, Thin Solid Films, 124, 323, (1985)

18. D.W. Butler, C.T.H. Stoddart and T.R. Stuart, J. Phys. D. $\underline{3}$, 877, (1970)

19. R. Jacobsson and B. Kruse, Thin Solid Films, $\underline{15}$, 71, (1977)

20. S.A. Varchenya and G.P. Upit, Thin Solid Films, $\underline{122}$, 59, (1984)

21. M.J. Mirtich, J. Vac. Sci. Technol., $\underline{18(2)}$, 186, (1981)

22. J. Salem and F. Sequeda, J. Vac. Sci. Technol., $\underline{18(2)}$, 149, (1981)

23. Quad Group, 2030 Alameda Padre Serra, Santa Barbara, CA 93103

24. B. Swaroop and I. Adler, J. Vac. Sci. Technol., $\underline{10}$, 503, (1973)

25. <u>Thin Films, Papers Presented at a Seminar of the American Society for Metals</u>, October 1963, American Society for Metals, (1964)

26. De Lodyguine, U.S. Patent 575002, (1893)

27. W.D. Grove, Phil. Trans., $\underline{B142}$, 87, (1852)

28. P. Sigmund, Phys. Rev., $\underline{184}$, 383, (1969)

29. R. Pohl and P. Pringsheim, Verhandl Deut Physik Ges, $\underline{14}$, 506, (1912)

30. L.I. Maissel and R. Glang, <u>Handbook of Thin Film Technology</u>, McGraw-Hill, (1970)

31. R.F. Bunshah et. al., <u>Deposition Technologies for Films and Coatings</u>, Noyes, (1982)

32. R.F. Bunshah, J. Vac. Sci. Technol. $\underline{B2(4)}$, (1984)

33. D.M. Mattox, Proc. Conf. Ion Plating and Allied Techniques, C.E.P. Consultants, Edinburgh, (1979)

34. P.A. Walley, Proc. Conf. Ion Plating and Allied Techniques, C.E.P. Consultants, Edinburgh, (1977)

35. D.G. Teer, Ibid

36. D.M. Mattox, J. Appl. Phys., $\underline{34}$, 2493, (1963)

37. S. Aisenberg and R.W. Chabot, J. Vac. Sci. Technol., $\underline{10(1)}$, 104, (1973)

38. D.L. Chambers and D.C. Carmichael, Research/Development Mag., _22_, 323, (1971)

39. B. Chapman, <u>Glow Discharge Processes</u>, John Wiley and Sons, (1980)

40. E. Nasser, <u>Fundamentals of Gaseous Ionization and Plasma Electronics</u>, Wiley Interscience, New York and London (1971)

41. W.D. Davis and T.A. Vanderslice, Phys. Rev., _131_, 219, (1963)

42. D.G. Teer, J. Adhesion, _8_, 289, (1977)

43. J. Rickards, Vacuum, _34_, (5), 559, (1984)

44. D.G. Armour, H. Vasilideh, F.A.H. Soliman and G. Carter, Vacuum, _34_, (1/2), 295, (1984)

45. P. Saulnier, A. Debhi and J. Machet, Vacuum, _34(8/9)_, 765, (1984)

46. A. Matthews and D.G. Teer, Thin Solid Films, _80_, 41, (1981)

47. B.A. Movchan and A.V. Demchishin, Phys. Met. Metallogr., _28_, 83, (1969)

48. J.A. Thornton, "Physical Vapor Deposition" in <u>Semiconductor Materials and Process Technologies</u>, ed. by G.E. McGuire, Noyes Publications, Park Ridge, NJ, (1984)

49. J.A. Thornton, Thin Solid Films, _40_, 335, (1977)

50. D.R. Gaskell, <u>Introduction to Metallurgical Thermodynamics</u>, McGraw-Hill, (1981), p. 167

51. Y. Enomoto and K. Matsubara, J. Vac. Sci. Technol., _12(4)_, 827, (1975)

52. E. Minni and H. Sundquist, Thin Solid Films, _80_, 55, (1981)

53. H.K. Pulker, W. Haag, M. Buhler and E. Moll, J. Vac. Sci. Technol., _A3(6)_, 2700, (1985)

54. W.D. Kingery, H.K. Bowen and D.R. Uhlmann, <u>Introduction to Ceramics</u>, John Wiley and Sons, (1960), p. 307

55. D.M. Mattox, Thin Solid Films, _124_, 3, (1985)

56. A. Piegari and E. Masetti, Thin Solid Films, _124_, 249, (1985)

57. P.A. Scott, Unpublished research

IX. APPENDICIES

APPENDIX A: Ion Energy Distribution

The derivations in this appendix are taken from Davis and Vanderslice [41] and Teer [35]; the reader is encouraged to consult these papers for a more complete explanation. The basis for the energy distribution is charge exhange collisions, with most of the ions originally being created in the negative glow. A linearly decreasing electric field across the cathode dark space is also assumed. For an ion to reach the cathode with an energy corresponding to a potential at some point in the dark space, Vx, it must undergo charge transfer at point x and not suffer any further collisions. The number of such ions is given by equation (A-1).

$$dN = (No/l)exp(-x/l)dx \qquad (A-1)$$

dN is the number of ions reaching the cathode with the specified energy, No is the number of ions created in the negative glow, l is the mean free path for charge transfer collisions, and x is the distance from the cathode. Using the linear field assumption, the distribution as a function of energy is arrived at (equation A-2);

$$\frac{VcdN}{NodV} = \frac{L}{l} \frac{1}{2(1-Vx/Vc)^{1/2}} \; exp-\{(L/l)[1-(1-Vx/Vc)^{1/2}]\} \quad (A-2)$$

where Vc is the cathode voltage. From this distribution, the total and average energies of the ions are then calculated by Teer (equations A-3,A-4).

$$Total \; Energy \; = \; \frac{NoVc2l}{L} \qquad (A-3)$$

119

$$\text{Average Energy} = \frac{Vc2I}{L} \quad (A-4)$$

Using these expressions for typical ion plating conditions, the average energy of the ions is approximately 10% of the maximum value and only 10% of the energy deposited at the cathode is due to ions.

APPENDIX B: Preparation of cross-section transmission
electron microscopy specimens

1.   Section film/substrate couple into 2 mm wide strips using
     slow speed diamond saw (figure B-1)

2.   Bond two strips together, with film sides in contact, using
     epoxy (figure B-2)

3.   Trim excess substrate, approximately 1 mm off of each side,
     from the sandwich (figure B-2)

4.   Place the sandwich in a 3.0 mm O.D. stainless steel tube,
     filling the empty space with epoxy (figue B-3)

5.   Cut a 0.600 mm disc from the tube

6.   Thin the disc to 0.150 mm using a dimpler with flattening
     tool (figure B-4)

7.   Thin the center of the disc to 0.050 mm using a dimpling tool
     (figure B-4)

8.   Ion mill the disc, using a liquid nitrogen cooled stage,
     until a perforation occurs at the interface

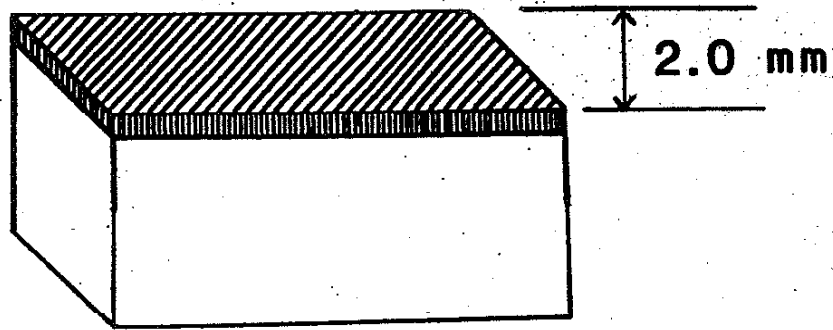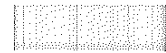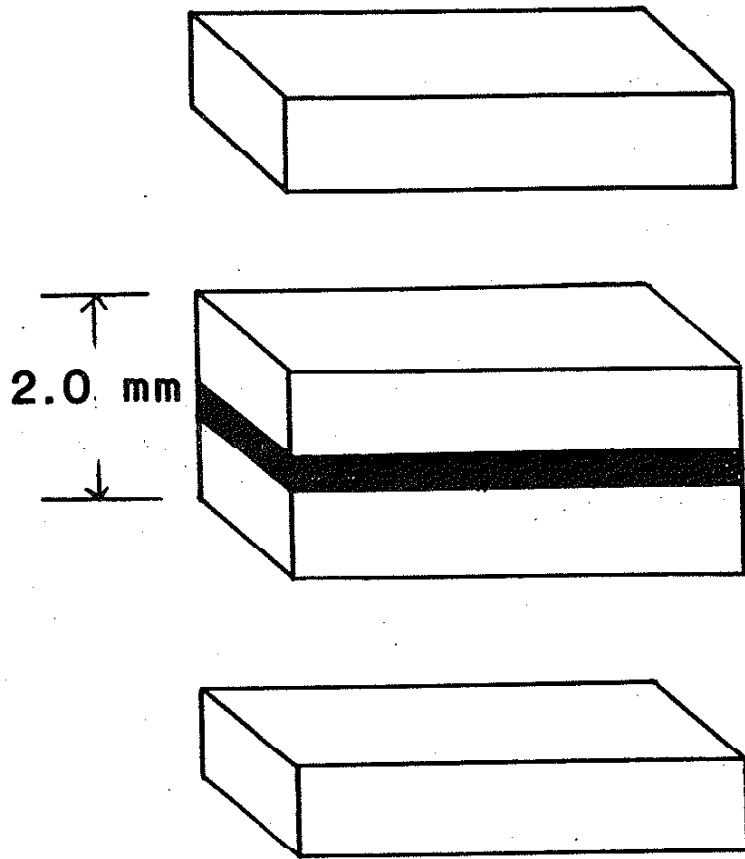9.   Carbon coat the sample to give conductivity
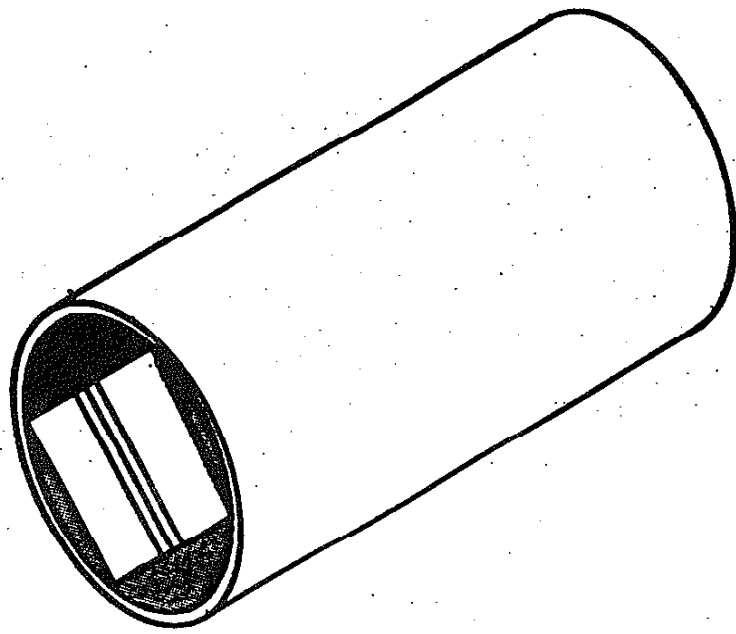
2.0 mm
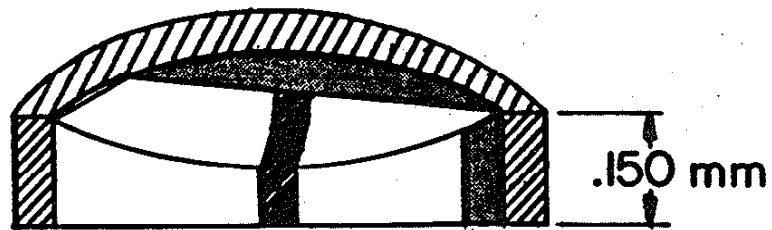
Figure B-1

2.0 mm

Figure B-2

Figure B-3

.150 mm

Figure B-4

APPENDIX C: Ion Implantation

In conjunction with the primary program of ion plating, efforts have been initiated into the areas of ion beam mixing and ion implantation.   The experiments were designed to compare the structure and properties of ion plated films, which are subjected to low energy (<5 kV) ion bombardment with ion beam mixed films, subjected to high energy (100 - 300 kV) ions.   The goal of the project was to produce an adherent, thermally stable metal/ceramic bond by mixing (producing a graded interface) thin nickel films (<1000 A) into a sputter cleaned cordierite surface via ion bombardment by high energy inert gas ions. Based on the adhesion results of the ion beam mixed specimens, a program of ion implantation of uncoated cordierite was begun in order to investigate the effects of ion bombardment on the structure, chemistry and properties of the ceramic. It is also planned to examine the properties of films deposited on these substrates after implantation.

Ion implantation of metals and semiconductors has been researched in great detail, yet the amount of information and understanding of the effects of high energy ions on ceramics is small in comparison.   For a thorough review of recent work on ion implantation, the reader is referred to the papaer by McHargue (International Metals Reviews, 1986, vol. 31, p. 49).   Enhanced adhesion via ion beam mixing is discussed in a paper by Baglin and Clark (Nuc. Inst. and Meth. in Phys. Res., vol. B7/8, p. 881).   Ion implantation of ceramics is often conducted to increase the strength of the substrate.   This may be acheived by

126

structural means, introducing a large amount of lattice damage –
up to the point of amorphization – into the surface; or by
chemical means, creating a supersaturated solid solution or
causing precipitation of a second phase. The increased strength
can be attributed to annihilation of flaws or introduction of a
compressive stress in the ceramic surface.

Mechanical strength of the film/substrate couples, as well
as the uncoated substrates was evaluated using a four point bend
test, with the processed side placed in tension. In addition,
the coated substrates were tested via the Sebastian adhesion
method described in the body of the thesis. All specimens were
implanted at the ion implantation facility of the Coordinated
Science Laboratory of the University of Illinois. Special thanks
are due to D. Shipley for his efforts in conducting the
implantations.

Adhesion results of the ion beam mixed films (table C-1)
proved to be inconclusive, since the as plated films posessed
good adhesion. The appearance of ceramic failures during
adhesion testing under certain implant conditions, as well as for
as received cordierite in the as plated condition, was cause for
alarm. As demonstrated in the four point bend results (table C-
2) the strength of the ceramic substrate can be degraded by ion
implantation. The strength may also be enhanced, if the
procedure is conducted under the correct parameters. Lower energy
and higher doses give the best results, based on the preliminary
indications. The use of nitrogen, as opposed to chromium, gives
better strength, but it has not yet been determined how the two

127

Table C-1: Adhesion results

Ion beam mixing

    Nickel film

    Cordierite substrate

    Krypton ions

<u>Failure mode</u>

Substrate	As Plated 1×10^{13}	100 keV 5×10^{13}	300 keV 5×10^{14} ($ions/cm^2$)	300 keV
As received ceramic	epoxy	epoxy	epoxy	
Polished no fails	epoxy	epoxy	epoxy	

128

Table C-2: Four point bend results

Chromium implantation

Breaking strength (MPa)

	Unimplanted	150 keV 1×10^{14}	150 keV 5×10^{15} ions/cm²
As received	175.0	103.7	
Polished	194.4	156.3	182.2

Nitrogen implantation

Breaking strength (MPa)

	200 keV 1×10^{15}	50 keV 5×10^{15}	295 keV, 100 keV 5×10^{15}, 1×10^{15} ions/cm²
Polished	157.3	204.9	204.0

ions would affect film growth on the implanted surface.

As stated, this program is still in the very early stages. Mechanical property analyses indicate we can indeed alter the structure, chemistry, and properties of the cordierite via direct high energy ion implantation. Promising conditions are being further evaluated in order to define an optimal processing window. Microstructural and microchemical investigations are being undertaken to better understand the effects of the implantation. Computer simulation via the TRIM code is also being initiated and will be compared to experimental results. By applying the techniques developed in examining ion plated metal/ceramic interfaces, an increased understanding of the process of ion implantation into cordierite, and the prospects for subsequently depositing adherent films on the implanted substrate, will be achieved.